PRL2 phosphatase enhances oncogenic FLT3 signaling via dephosphorylation of the E3 ubiquitin ligase CBL at tyrosine 371

Hongxia Chen[1,2,16#], Yunpeng Bai[3#], Michihiro Kobayashi[4], Shiyu Xiao[2], Wenjie Cai[2,4], Sergio Barajas[2,4], Sisi Chen[4], Jinmin Miao[3], Frederick Nguele Meke[3], Sasidhar Vemula[4], James P. Ropa[5], James M. Croop[4], H. Scott Boswell[6], Jun Wan[7], Yuzhi Jia[8], Huiping Liu[8,9], Loretta S. Li[9,10], Jessica K. Altman[2,9], Elizabeth A. Eklund[2, 9, 11], Peng Ji[9,12], Wei Tong[13], Hamid Band[14], Danny T. Huang[15], Leonidas C. Platanias[2,9,11], Zhong-Yin Zhang[3*], and Yan Liu[2,9*]

[1]Department of Hematology and Oncology, Chongqing University Three Gorges Hospital, Chongqing, China; [2]Department of Medicine, Feinberg School of Medicine, Northwestern University, Chicago, IL; [3]Department of Medicinal Chemistry and Molecular Pharmacology, Center for Cancer Research, and Institute for Drug Discovery, Purdue University, West Lafayette, IN; [4]Department of Pediatrics, Herman B Wells Center for Pediatric Research, Indiana University School of Medicine, Indianapolis, IN; [5]Department of Microbiology and Immunology, Indiana University School of Medicine, Indianapolis, IN; [6]Department of Medicine, Indiana University School of Medicine, Indianapolis, IN; [7]Department of Medical Genetics, Indiana University, Indianapolis, IN; [8]Department of Pharmacology, Feinberg School of Medicine, Northwestern University, Chicago, IL; [9]Robert H. Lurie Comprehensive Cancer Center, Chicago, IL; [10]Department of Pediatrics, Feinberg School of Medicine, Northwestern University, Chicago, IL; [11]Department of Medicine, Jesse Brown VA Medical Center, Chicago, IL; [12]Department of Pathology, Feinberg School of Medicine, Northwestern University, Chicago, IL; [13]Children's Hospital of Philadelphia, University of Pennsylvania School of Medicine, Philadelphia, PA; [14]Department of Genetics, University of Nebraska Medical Center, Omaha, NB; [15]Cancer Research UK Beatson Institute and Institute of Cancer Sciences, University of Glasgow, Glasgow, United Kingdom; [16]School of Medicine, Chongqing University, Chongqing, China.

[#] These authors contributed equally to the paper

*Correspondence: zhang-zy@purdue.edu; yan.liu@northwestern.edu

KEY POINTS

Genetic and pharmacological inhibition of PRL2 significantly reduce the burden of FLT3-ITD-driven leukemia and extend leukemic mice survival.

PRL2 dephosphorylates CBL at tyrosine 371 and blocks CBL-mediated FLT3 ubiquitination and degradation, leading to enhanced STAT5, AKT, and ERK signaling in leukemia cells.

Abstract

Acute myeloid leukemia (AML) is an aggressive blood cancer with poor prognosis. FLT3 is one of the major oncogenic receptor tyrosine kinases aberrantly activated in AML. While protein tyrosine phosphatase PRL2 is highly expressed in some subtypes of AML compared to normal human hematopoietic stem and progenitor cells (HSPCs), the mechanisms by which PRL2 promotes leukemogenesis are largely unknown. We discovered that genetic and pharmacological inhibition of PRL2 significantly reduce the burden of FLT3-ITD-driven leukemia and extend the survival of leukemic mice. Further, we found that PRL2 enhances oncogenic FLT3 signaling in leukemia cells, promoting their proliferation and survival. Mechanistically, PRL2 dephosphorylates the E3 ubiquitin ligase CBL at tyrosine 371 and attenuates CBL-mediated ubiquitination and degradation of FLT3, leading to enhanced FLT3 signaling in leukemia cells. Thus, our study reveals that PRL2 enhances oncogenic FLT3 signaling in leukemia cells through dephosphorylation of CBL and will likely establish PRL2 as a novel druggable target for AML.

Introduction

Acute myeloid leukemia (AML) is an aggressive blood cancer with poor prognosis.[1-3] Some human leukemia cells depend on aberrant receptor tyrosine kinase activation and the downstream effectors for proliferation and survival.[4-5] FMS-like tyrosine kinase receptor-3 (FLT3) is one of the major oncogenic receptor tyrosine kinases aberrantly activated in AML.[6-7] Activating *FLT3* mutations, including internal tandem duplications in *FLT3* (*FLT3-ITD*), are seen in approximately 30% of AML patients and confer a poor prognosis.[6-7] Despite substantial efforts devoted to the development of FLT3 inhibitors, the effectiveness of these inhibitors as a single agent in AML has been limited and development of drug resistance in leukemia patients is always a concern. [6-9] The resistance to targeted therapies seen in AML patients may be associated with a rare population of leukemia-initiating cells (LICs) or leukemia stem cells (LSCs) that are capable of self-renewal and initiating leukemia.[10-14]

The CBL family E3 ubiquitin ligases, including CBL and CBL-b, are responsible for the ubiquitination and degradation of FLT3 in hematopoietic cells.[15] CBL is a tumor suppressor in hematological malignancies. Indeed, loss of both *CBL* and *CBL-b* results in fetal myeloproliferative neoplasms (MPN) in mice.[16-18] Both somatic and germline *CBL* mutations are frequently found in myeloid malignancies, including juvenile myelomonocytic leukemia (JMML), myelodysplastic syndromes (MDS), MPN, and AML.[19-22] In response to cytokine stimulation, CBL is phosphorylated and activated.[15] However, how CBL phosphorylation is downregulated in leukemia cells is largely unknown.

The **p**hosphatases of **r**egenerating **l**iver (PRL1, 2 and 3) are members of the protein tyrosine phosphatase (PTP) family that are being pursued as biomarkers and therapeutic targets in human cancers.[23-26] PRL2, also known as PTP4A2, is essential for hematopoietic stem and progenitor cell (HSPC) proliferation and promotes AML1-ETO-induced leukemia.[27, 28] In addition, PRL2 regulates T cell development and promotes oncogenic NOTCH1-induced T-cell leukemia.[29, 30] While *PRL2* is highly expressed in some subtypes of AML compare to normal human HSPCs,[28] the mechanisms by which PRL2 promotes leukemogenesis are unclear. In this study, we discovered that PRL2

dephosphorylates CBL at tyrosine 371 and inhibits its E3 ubiquitin ligase activity toward FLT3, leading to decreased ubiquitination of FLT3, and activation of FLT3-induced downstream signaling pathways in leukemia cells.

Methods

Detailed methodology is provided in the Supplemental Information (Available on the Blood Web site).

Mice

Wild type C57BL/6 (CD45.2^{+}), B6.SJL (CD45.1^{+}), C3H/HeJ, and *Flt3*$^{+/ITD}$ mice were purchased from the Jackson Laboratories. *Prl2*$^{+/+}$, *Prl2*$^{-/-}$, *Flt3*$^{+/ITD}$, *Flt3*$^{+/ITD}$*Prl2*$^{-/-}$, *Flt3*$^{ITD/ITD}$ and *Flt3*$^{ITD/ITD}$*Prl2*$^{-/-}$ mice were maintained in the Indiana and Northwestern University Animal Facility and kept in Thorensten units with filtered germ-free air. Embryonic day 14.5 (E14.5) fetal liver cells (*Prl2*$^{+/+}$ and *Prl2*$^{-/-}$) were isolated from pregnant *Prl2*$^{+/-}$ female mice that were mated with *Prl2*$^{+/-}$ *male* mice. The Institutional Animal Care and Use Committee (IACUC) of Indiana University School of Medicine and Northwestern University Feinberg School of Medicine approved all experimental procedures.

Statistical Analysis

The animal sample size was based on previous studies evaluating the roles of PRL2 in leukemia and POWER analysis.[26,27] Using Chi-Square analysis, 7 mice per group will provide 80% POWER in detecting difference with 95% difference. Gehan-Breslow-Wilcoxon test was used for Kaplan-Meier survival curves. Other data were analyzed by paired or unpaired t test or analysis of variance for nonlinear distributions using GraphPad Prizm 9. Results are expressed as the mean ± standard error of the mean (SEM) for at least triplicate experiments. P values of < 0.05 were regarded as statistically significant which was calculated by GraphPad Prism9. *p<0.05, **p<0.01, ***p < 0.001, ****p < 0.0001. Further details about methods are available in supplementary information.

Data Sharing Statement

RNA-seq data are available at GEO under accession number GSE208136.

Results

FLT3 mutated AML patients with high *PRL2* expression have reduced overall survival

To determine the role of PRL2 (PTP4A2) in the pathogenesis of human AML, we first analyzed the published TCGA (https://www.cancer.gov/about-nci/organization/ccg/research/structural-genomics/tcga) dataset and found that PRL2 expression is higher in intermediate and poor risk AML compared to favorable risk AML (Figure 1A). PRL2 expression is also higher in dead AML patients compared to AML patients that are alive (Figure 1B). We then analyzed the dataset from cBioPortal (https://www.cbioportal.org) and found that *PRL2* levels are higher in patients with cytogenetic and central nerve system (CNS) relapse (Figure 1C; supplemental Figure 1A). We defined *PRL2* expression above median as high *PRL2* expression group and below median as low *PRL2* expression group. Notably, AML patients with high *PRL2* expression have reduced overall survival compared to AML patients with low *PRL2* expression (Supplemental Figure 1B). In AML bearing poor cytogenetic risk, patients with high *PRL2* expression have reduced overall survival compared to patients with low *PRL2* expression (Figure 1D; supplemental Figure 1C-D). Next, we performed DEG (differentially expressed gene) analysis to compare gene expression in a subset of AML patients with high or low *PRL2* expression. There are 790 genes upregulated and 948 genes downregulated in AML patients with high *PRL2* expression (Figure 1E). Gene Set Enrichment Analysis (GSEA) revealed that AML, AML prognosis, leukemia stem cell (LSC), and hematopoietic stem cell (HSC) gene signatures are enriched in AML patients with high *PRL2* expression (Figure 1F). In addition, pathways associated with FLT3 as well as its downstream effectors, including STAT5A, PI3K/AKT, and ERK1/ERK2, are enriched in *PRL2* high group (Figure 1G-H).

We then analyzed *PRL2* expression in AML patients with or without *FLT3* mutations using GSE15434 and cBioPortal dataset and found that AML patient with *FLT3* mutations have higher *PRL2* expression

compared to AML patients negative for *FLT3* mutations (Figure 1I; supplemental Figure 1E). In AML patients without *FLT3* mutations, *PRL2* expression did not appear to affect overall survival (Supplemental Figure 1F). However, in *FLT3* mutation positive AML, patients with high *PRL2* expression have reduced overall survival compared to patients with low *PRL2* expression (Figure 1J). Taken together, these clinical data suggest that high *PRL2* expression may be a prognostic marker in *FLT3*-mutated AML.

PRL2 deficiency alters FLT3 mediated gene transcription in murine hematopoietic stem and progenitor cells

To gain insights into the molecular mechanisms underlying the role of PRL2 in hematopoietic stem and progenitor cells (HSPCs), we performed RNA-seq analysis to compare gene expression in $Prl2^{+/+}$ and $Prl2^{-/-}$ E14.5 (Embryonic day 14.5) fetal liver cells which are enrich with HSPCs. Approximately 400 genes were significantly downregulated, and 75 genes were significantly upregulated in $Prl2^{-/-}$ fetal liver cells, respectively (Figure 2A). We then employed GSEA analysis to group potential PRL2 target genes into specific pathways important for HSPC behavior. Notably, long-term hematopoietic stem cells, receptor tyrosine kinase signaling, PI3K/AKT signaling, and ERK signaling gene signatures were significantly downregulated in *Prl2* null fetal liver cells (Figure 2B). In addition, receptor regulator activity, receptor complex, positive regulation of receptor tyrosine kinase signaling, and positive regulation of ERK signaling gene signatures were significantly down regulated in *Prl2* null fetal liver cells (Figure 2C-D). We utilized STRING 11.5 to perform protein association network analysis on genes downregulated in *Prl2* null fetal liver cells and observed strong interconnection between downregulated genes with FLT3 and its downstream proteins in *Prl2* null fetal liver cells (Figure 2E). We confirmed that the expression of genes interacting with the FLT3 signaling pathway was downregulated in *Prl2* null fetal liver cells (Figure 2F), *Prl2* null fetal liver Kit^+ cells (supplemental Figure 2A), as well as *Prl2* null bone marrow Lin^- cells (Figure 2G). Loss of *Prl2* significantly decreased AKT, STAT5 and ERK

phosphorylation in fetal liver cells (Figure 2H; supplemental Figure 2B) and bone marrow Lin^- cells (Figure 2I; supplemental Figure 2C).

Loss of *Prl2* decreases the self-renewal capability of FLT3-ITD positive hematopoietic stem and progenitor cells

To determine the role of PRL2 in FLT3-ITD-mediated hematopoietic cell proliferation, we introduced wild-type (WT) FLT3 or FLT3-ITD mutant into Lin^- cells purified from WT and *Prl2* null mice and found that *Prl2* null Lin^- cells expressing FLT3-ITD exhibit decreased proliferation compared to that of the WT cells both in the absence of cytokines and in the presence of FLT3 ligand (supplemental Figure 2D). As expected, ectopic expression of FLT3-ITD increased the colony formation of WT HSPCs (supplemental Figure 2E). While *Prl2* deficiency did not affect the colony formation of HSPCs expressing WT FLT3, loss of *Prl2* decreased the colony formation of HSPCs expressing FLT3-ITD (supplemental Figure 2E). These findings suggest that PRL2 is important for FLT3-ITD-mediated hematopoietic cell hyperproliferation.

To further determine the impact of PRL2 on oncogenic FLT3 signaling, we have generated $Flt3^{+/ITD}Prl2^{-/-}$ and $Flt3^{ITD/ITD}Prl2^{-/-}$ mice.[32] $Prl2^{-/-}$ mice show decreased body size as we previously reported;[28,33] however, expression of FLT3-ITD did not rescue the body size defect seen in the $Prl2^{-/-}$ mice (supplemental Figure 3A). To determine the impact of Prl2 on hematopoiesis, we first analyzed the peripheral blood (PB) and bone marrow (BM) of 8- to 12-week-old $Prl2^{+/+}$, $Prl2^{-/-}$, $Flt3^{+/ITD}$, $Flt3^{+/ITD}Prl2^{-/-}$, $Flt3^{ITD/ITD}$, and $Flt3^{ITD/ITD}Prl2^{-/-}$ mice. $Flt3^{ITD/ITD}$ mice show increased white blood cell (WBC) counts as reported,[32] whereas loss of *Prl2* brought WBC counts back to normal (supplemental Figure 3B). Both $Flt3^{ITD/ITD}$ and $Flt3^{ITD/ITD}Prl2^{-/-}$ mice are anemic, manifested by decreased red blood cell (RBC) counts and reduced hemoglobin (HGB) levels in peripheral blood (supplemental Figure 3C-D). In addition, $Flt3^{ITD/ITD}$ mice displayed decreased levels of platelets but increased levels of basophil and monocyte counts (supplemental Figure 3E-H). There is increased number of myeloid cells in PB of

Flt3$^{ITD/ITD}$ mice; however, loss of *Prl2* mitigated this effect (supplemental Figure 3I). Both *Flt3*$^{+/ITD}$ and *Flt3*$^{ITD/ITD}$ mice displayed increased BM cellularity compared to WT mice, whereas loss of *Prl2* brought BM cellularity back to normal (supplemental Figure 3J). There are decreased number of B cells but increased number of myeloid cells in the BM of *Flt3*$^{ITD/ITD}$ mice (supplemental Figure 3K-M). Loss of *Prl2* significantly reduced the number of myeloid cells in the FLT3-ITD background (supplemental Figure 3M).

We next examined the number of primitive hematopoietic stem and progenitor cells in the BM of *Prl2*$^{+/+}$, *Prl2*$^{-/-}$, *Flt3*$^{+/ITD}$, *Flt3*$^{+/ITD}$*Prl2*$^{-/-}$, *Flt3*$^{ITD/ITD}$, and *Flt3*$^{ITD/ITD}$*Prl2*$^{-/-}$ mice. *Flt3*$^{ITD/ITD}$ mice have increased number of long-term hematopoietic stem cells (LT-HSCs), multipotent progenitor cells (MPPs), and Lin^{-}Sca1^{+}Kit^{+} cells (LSKs) in their BM, whereas loss of *Prl2* brought the numbers of hematopoietic stem and progenitor cells (HSPCs) back to WT level (Figure 3A, C-D; supplemental Figure 3N). While loss of *Prl2* decreases the number of ST-HSCs, *Prl2* deficiency has modest impact on ST-HSCs in FLT3-ITD background (Figure 3B). We then performed methylcellulose colony-forming unit (CFU) assays to quantify myeloid progenitor cells. While *Flt3*$^{ITD/ITD}$ BM cells show increased colony formation, loss of *Prl2* significantly decreased their ability to form colonies *in vitro* (Figure 3E), suggesting that PRL2 is important for FLT3-ITD-mediated enhanced hematopoietic cell proliferation.

To examine whether *Prl2* deficiency affects *Flt3*$^{+/ITD}$ HSPC function *in vivo*, we performed serial competitive BM transplantation assays using *Prl2*$^{+/+}$, *Prl2*$^{-/-}$, *Flt3*$^{+/ITD}$, and *Flt3*$^{+/ITD}$*Prl2*$^{-/-}$ BM cells (CD45.2^{+}). Equal numbers of donor and competitor BM cells were transplanted into lethally irradiated recipient mice (supplemental Figure 4A). Sixteen weeks after primary transplantation, we found that loss of *Prl2* significantly decreases the engraftment of *Flt3*$^{+/ITD}$ BM cells (Figure 3F). Recipient mice repopulated with *Flt3*$^{+/ITD}$ BM cells showed increased levels of WBC counts, whereas loss of *Prl2* in the *Flt3*$^{+/ITD}$ background brought WBC counts back to normal (supplemental Figure 4B-C).

Analysis of the BM revealed a striking increase in the number of phenotypically defined MPPs and LSKs in the recipients repopulated with *Flt3*$^{+/ITD}$ BM cells, whereas the number of LT-HSCs and short-term hematopoietic stem cells (ST-HSCs) are normal (Figure 3G-H). Loss of *Prl2* significantly reduced the number of MPPs and LSKs in the *Flt3*$^{+/ITD}$ background (Figure 3I-J; supplemental Figure 4D). We then transplanted 3 × 10^6 BM cells isolated from the primary recipient mice repopulated with *Prl2*$^{+/+}$, *Prl2*$^{-/-}$, *Flt3*$^{+/ITD}$, and *Flt3*$^{+/ITD}$*Prl2*$^{-/-}$ BM cells into lethally irradiated secondary recipients (supplemental Figure 4E). Sixteen weeks after transplantation, *Flt3*$^{+/ITD}$*Prl2*$^{-/-}$ cells continued to show decreased repopulating ability (Figure 3K). Recipient mice repopulated with *Flt3*$^{+/ITD}$ BM cells showed increased levels of WBC counts, whereas loss of *Prl2* in the *Flt3*$^{+/ITD}$ background brought WBC counts back to normal (supplemental Figure 4F). Interestingly, we observed increased lymphocyte counts in the secondary recipients repopulated with *Flt3*$^{+/ITD}$ BM cells and loss of *Prl2* mitigated the effect (supplemental Figure 4G). Strikingly, loss of *Prl2* significantly decreased the number of *Flt3*$^{+/ITD}$ ST-HSCs, MPPs, and LSKs, but not LT-HSCs in the BM of secondary recipient mice (Figure 3L-O; supplemental Figure 4H). Recipient mice repopulated with *Flt3*$^{+/ITD}$ BM cells showed enlarged spleen and loss of *Prl2* rescued the defect (supplemental Figure 4I-J).

PRL2 is important for FLT3-ITD-induced myeloid proliferative neoplasm in mice

Both *Flt3*$^{+/ITD}$ and *Flt3*$^{ITD/ITD}$ mice develop MPN with monocytic features.[32] *Flt3*$^{+/ITD}$ and *Flt3*$^{ITD/ITD}$ mice displayed dose-dependent development of progressive splenomegaly, whereas loss of *Prl2* significantly reduced splenomegaly seen in *Flt3*$^{+/ITD}$ and *Flt3*$^{ITD/ITD}$ mice (Figure 4A-B). While there are increased number of LSKs in the spleen of *Flt3*$^{+/ITD}$ and *Flt3*$^{ITD/ITD}$ mice, loss of *Prl2* mitigated the effect (Figure 4C).

To determine the hematopoietic cell intrinsic effect of PRL2 on FLT3-ITD induced MPN, we transplanted 3 x 10^6 BM cells (CD45.2$^+$) isolated from *Prl2*$^{+/+}$, *Prl2*$^{-/-}$, *Flt3*$^{+/ITD}$, *Flt3*$^{+/ITD}$*Prl2*$^{-/-}$, *Flt3*$^{ITD/ITD}$, and *Flt3*$^{ITD/ITD}$*Prl2*$^{-/-}$ mice into lethally irradiated recipient mice (CD45.1$^+$). All recipient

mice repopulated with *Flt3*$^{ITD/ITD}$ BM cells developed MPN and died within 60 weeks after transplantation; however, loss of *Prl2* significantly extended the survival of *Flt3*$^{ITD/ITD}$ mice, with 50% of mice still alive at 73 weeks following transplantation (Figure 4D). *Prl2* deficiency rescued anemia seen in recipient mice repopulated with *Flt3*$^{ITD/ITD}$ BM cells, manifested by increased RBC counts and HGB levels in PB (Figure 4E-F; supplemental Figure 5A-B). In addition, loss of *Prl2* rescued myeloid expansion seen in PB of *Flt3*$^{ITD/ITD}$ mice (supplemental Figure 5C-G). Flow cytometric analysis further confirmed the expansion of Mac1^{+}Gr1^{+} myeloid cells in PB of recipient mice repopulated with *Flt3*$^{+/ITD}$ or *Flt3*$^{ITD/ITD}$ BM cells and loss of *Prl2* rescued the defect observed in the *Flt3*$^{ITD/ITD}$ group (Figure 4G-H). Recipient mice repopulated with *Flt3*$^{+/ITD}$ and *Flt3*$^{ITD/ITD}$ BM cells developed MPN, manifested by splenomegaly and infiltration of maturing myeloid hyperplasia in bone marrow, spleen, and liver as well as accumulation of myeloid blast cells in PB; however, these abnormalities were significantly reduced in *Flt3*$^{+/ITD}$*Prl2*$^{-/-}$ and *Flt3*$^{ITD/ITD}$*Prl2*$^{-/-}$ mice (Figure 4I; supplemental Figure 5H). Recipient mice repopulated with *Flt3*$^{ITD/ITD}$ BM cells displayed splenomegaly, whereas loss of *Prl2* significantly reduced splenomegaly seen in *Flt3*$^{ITD/ITD}$ mice (Figure 4J).

To complement our murine studies, we ectopically expressed WT PRL2 or a catalytically inactive mutant (PRL2-CSDA, where the active site C101 and D69 were mutated to S and A, respectively) in a murine hematopoietic progenitor cell line 32D and performed *in vitro* and *in vivo* experiments.[30, 34] We found that ectopic expression of PRL2-CSDA decreases the proliferation of 32D cells expressing FLT3-ITD (Figure 4K). We also transplanted transduced 32D cells into sublethally irradiated C3H/HeJ mice and monitor their survival. While ectopic expression of PRL2 had no effect on the survival of C3H/HeJ mice transplanted with FLT3-ITD expressing 32D cells, expression of PRL2-CSDA significantly extended the survival of C3H/HeJ mice (Figure 4L).

Genetic and pharmacological inhibition of PRL2 decreases leukemia burden and extends the survival of mice transplanted with human leukemia cell lines

MV-4-11, MOLM-13, and K562 are human AML cell lines.[35] To examine the impact of PRL2 deficiency on human leukemia cell proliferation, we have developed two shRNAs targeting different regions of human *PRL2*.[27, 30] Both shRNAs can efficiently decrease PRL2 proteins in MV-4-11 cells (Figure 5A). We focused our studies using one of the PRL2 shRNA and found that knockdown of PRL2 decreases the colony formation of MV-4-11, MOLM-13, and K562 cells (Figure 5B and supplemental Figure 6A-C). To determine the impact of PRL2 deficiency on leukemia development *in vivo*, we transplanted 3 x 10^6 MV-4-11 or MOLM-13 cells expressing control or PRL2 shRNA into sublethally irradiated NSG mice and monitored their survival. We found that loss of PRL2 significantly extended the survival of recipient mice transplanted with MV-4-11 or MOLM-13 cells (Figure 5C; supplemental Figure 6D). In addition, we found genetic inhibition of PRL2 significantly decreases the engraftment of MV-4-11 cells in PB, BM, and spleen of recipient mice (Figure 5D). Furthermore, knockdown of PRL2 significantly decreased splenomegaly seen in recipient mice transplanted with MV-4-11 cells (Figure 5E-F).

To further substantiate the PRL2 knockdown results, we also utilized compound 43,[31] a small molecule PRL inhibitor (PRLi) that blocks PRL trimerization, which is essential for PRL function.[31, 36, 37] Consistent with previous findings,[31] PRLi treatment reduces the colony formation of MV-4-11, MOLM-13, and K562 cells (Figure 5G; supplemental Figure 6E-F). To determine the efficacy of PRLi on human leukemia cells *in vivo*, we transplanted luciferase-labeled MV-4-11 cells into sublethally irradiated NSG via tail vein injection. One week after the transplantation, we treated NSG mice with vehicle (10% DMSO) or PRLi (25 mg/kg, I.P.) daily for three weeks. Leukemia burden in NSG mice was monitored via bioluminescence imaging weekly. Serial imaging of luminescence showed that PRLi treatment dramatically decreases leukemia burden compared with the control group (Figure 5H). The radiance of the NSG mice was significantly reduced after exposure to PRLi (Figure 5I). Furthermore, PRLi substantially extended the survival of NSG mice transplanted with human leukemia cells (Figure 5J).

PRLi also considerably decreased the engraftment of human leukemia cells in PB, BM, and spleen of NSG mice (Figure 5K). PRLi treatment significantly reduced the size and weight of spleen of NSG mice (Figure 5L-M). Finally, we found that PRLi is specific for PRL2 as it does not affect the colony formation of MV-4-11, MOLM-13, and K562 cells expressing a shRNA targeting PRL2 (supplemental Figure 6G). Further, PRLi inhibits the proliferation of MV-4-11 and MOLM-13 cells expressing PRL2, but not MV4-11 and MOLM-13 cells expressing PRL2-CSDA (Supplementary Figure 6H).

Pharmacological inhibition of PRL2 reduces leukemia burden and extends the survival of mice transplanted with primary human AML cells

PRLi decreases the proliferation of primary human AML cells *in vitro* in a dosage-dependent manner (Figure 6A). In addition, PRLi treatment decreases the colony formation of primary human AML cells with or without FLT3 mutations (Figure 6B). PRLi treatment also arrested primary AML cells with FLT3-ITD mutation at the G0/G1 phase of the cell cycle and decreased the percentage of cells in S or G2M phase (Figure 6C; supplemental Figure 6I). Further, PRLi treatment significantly increased the apoptosis of primary human AML cells with FLT3-ITD mutation (Figure 6D; supplemental Figure 6J).

To determine the efficacy of PRLi on primary human leukemia cells *in vivo*, we generated two patient-derived xenograft (PDX) models of FLT3-ITD positive AML in NSGS mice. 12-16 weeks post primary transplantation, we confirmed engraftment of human $CD45^+$ ($huCD45^+$) AML cells in NSGS mice (data not shown) and generated secondary recipients for drug administration. After confirmation of human leukemia cell engraftment in peripheral blood of NSG mice (>1% human $CD45^+$ cells), NSG mice were treated with vehicle (10% DMSO) or PRLi (25 mg/kg, I.P.) daily for three weeks. PRLi substantially extended the survival of NSG mice transplanted with human $CD45^+$ leukemia cells (Figure 6E; supplemental Figure 6K). PRLi also considerably decreased the engraftment of human $CD45^+$ leukemia

297 cells in PB, BM, and spleen of NSG mice at the end point of treatment (Figure 6F; supplemental Figure
298 6L).

299 **PRL2 is a positive mediator of oncogenic FLT3 signaling in murine hematopoietic cells and**
300 **human leukemia cells**

301 To determine the impact of PRL2 on FLT3 signaling, we examined STAT5, AKT, and ERK
302 phosphorylation and found that loss of *Prl2* decreases STAT5, AKT, and ERK phosphorylation in both
303 *Flt3*$^{+/ITD}$ and *Flt3*$^{ITD/ITD}$ BM cells (Figure 6G). These observations suggest that PRL2 is a positive
304 mediator of FLT3-ITD signaling in hematopoietic cells. To determine the impact of PRL2 deficiency on
305 FLT3 signaling in leukemia cells, we found that knock down of *PRL2* significantly decreases pFLT3,
306 FLT3 expression, AKT, ERK and STAT5 phosphorylation in MV-4-11 cells (Figure 6H, left panel). In
307 addition, we showed that PRLi treatment also decreases pFLT3, FLT3 expression, AKT, ERK, STAT5,
308 STAT3 and MEK phosphorylation in MV-4-11 cells (Figure 6H right panel; supplemental Figure 7A).
309 Moreover, we observed decreased pFLT3, FLT3 expression, phosphorylation of AKT, STAT5, STAT3,
310 STAT1 and MEK in K562 cells following PRLi treatment (supplemental Figure 7B), but there was no
311 change in the levels of BCR-ABL, BCR, and c-ABL (supplemental Figure 7C). We also found that
312 PRLi treatment reduces FLT3 expression and decreases the phosphorylation of AKT, ERK, and STAT5
313 in U937 cells expressing WT FLT3 or FLT3-ITD (supplemental Figure 7D). We found that decreased
314 phosphorylation of AKT, STAT5, and ERK in MV4-11 cells expressing shPRL2 isolated from NSG
315 mice at 4 weeks following transplantation (Figure 6J left; supplemental Figure 7E left). Notably, we
316 observed decreased phosphorylation of AKT, STAT5, and ERK in MV4-11 and primary human AML
317 cells isolated from NSG mice following three weeks of PRLi treatment (Figure 6J-K; supplemental
318 Figure 7E). While PTEN is a negative regulator of the AKT signaling pathway,[28] PRLi treatment did not
319 affect PTEN expression in MV4-11 cells (supplemental Figure 7F). Finally, we showed that PRLi is
320 synergic with FLT3 inhibitor AC220 or Gilteritinib in inhibiting the proliferation in MV-4-11 cells
321 (supplemental Figure 7G).

PRL2 associates with and dephosphorylates CBL at tyrosine 371 in leukemia cells

To investigate the mechanism by which PRL2 promotes FLT3 signaling, we determined the effect of PRL2 inhibition on FLT3 stability. We discovered that both knockdown of PRL2 and PRLi treatment can lead to a reduction in FLT3 protein level as a result of a decrease in FLT3 half-life in MV-4-11 cells (Figure 7A; supplemental Figure 8A). In line with this observation, we found that both knockdown of PRL2 and PRLi treatment increase FLT3 ubiquitination in MV-4-11 cells (Figure 7B; supplemental Figure 8B).

To understand how does PRL2 promote FLT3 stabilization, we carried out substrate trapping experiments to identify potential PRL2 substrates in leukemia cells. To that end, we utilized the GST-tagged PRL2-CSDA mutant, which is competent for substrate binding but unable to catalyze substrate turnover.[34, 38] Indeed, we found that PRL2-CSDA shows enhanced association with CBL, FLT3, PLCγ, and SHP2 compared to wild-type PRL2 in MV-4-11 cells (Figure 7C). We confirmed that PRL2 associates with FLT3 and CBL in MV-4-11 cells using co-immunoprecipitation (Co-IP) assays (Figure 7D). We also found that PRL2 and CBL co-localizes in MV-4-11 (Figure 7E) and U2OS cells (supplemental Figure 8C). Given that CBL is an E3 ubiquitin ligase which is responsible for ubiquitination and degradation of FLT3 in hematopoietic cells,[15] these findings suggest that CBL may be a PRL2 substrate.

CBL becomes phosphorylated on several tyrosine residues following cytokine stimulation (supplemental Figure 8D). To determine whether CBL can serve as a substrate for PRL2, we expressed PRL2 in 293 cells and found that ectopic PRL2 expression decreases CBL tyrosine phosphorylation in 293 cells (Figure 7F). Conversely, knockdown of PRL2 increases CBL tyrosine phosphorylation in MV-4-11 cells (Figure 7G). CBL becomes activated upon Tyrosine 371 phosphorylation, which enables it to

target receptor protein tyrosine kinases for ubiquitin-mediated degradation.[15, 22, 39-41] Indeed, we found that knockdown of PRL2 increases CBL phosphorylation at tyrosine 371, whereas the levels of CBL phosphorylation at tyrosine 700, 731, and 774 were not affected by PRL2 inhibition in MV-4-11 cells (Figure 7H). We detected that ectopic expression of the catalytically inactive PRL2-CSDA mutant increases CBL phosphorylation at tyrosine 371 in MV-4-11 cells (Figure 7I). Further, we found that PRLi treatment increases CBL phosphorylation at tyrosine 371 in MV-4-11 cells (supplemental Figure 8E).

To further examine the enzyme-substrate interaction between PRL2 and CBL at the molecular level, we utilized APEX2 proximity labeling, which is a widely used method for rapid covalent labeling of neighboring proteins within a 10–20 nm radius of a protein of interest in living cells.[42-44] To that end, APEX2-PRL2 fusion protein was used to perform proximity labeling to identify its interacting proteins. To our satisfaction, we identified CBL as a PRL2 neighboring protein, but not the nonphosphorylatable CBL^{Y371F} mutant, in live cells (Figure 7J). Consistently, the PRL2-CSDA substrate trapping mutant shows enhanced association with CBL compared to the CBL^{Y371F} mutant in both HeLa and 293 cells (Figure 7K-L). Notably, CBL expression is correlated with PRL2 expression in human leukemia patients (supplemental Figure 8F). Collectively, the data presented above demonstrate that CBL is a substrate of PRL2 and that PRL2 associates with and dephosphorylates CBL at tyrosine 371 in leukemia cells. It follows that dephosphorylation of CBL at tyrosine 371 by PRL2 blocks CBL-mediated FLT3 ubiquitination and degradation, leading to heightened FLT3 signaling in leukemia cells.

Discussion

Members of the PTP family dephosphorylate target proteins and counter the activities of protein tyrosine kinases to control the strength and duration of tyrosine phosphorylation mediated cellular signaling.[45, 46] FLT3 is a major oncogenic receptor tyrosine kinase aberrantly activated in leukemia.[6, 7] PRL2 is known

to be overexpressed in some subtypes of AML.[27] In the present study, we demonstrate that PRL2 enhances oncogenic FLT3 signaling and promotes leukemia cell proliferation and survival. We further establish that PRL2 dephosphorylates CBL at tyrosine 371 and inhibits it's E3 ligase activity toward FLT3, leading to decreased ubiquitination and degradation of FLT3, thereby activating its downstream signaling pathways in leukemia cells. Finally, we also show that genetic and pharmacological inhibition of PRL2 significantly reduce the burden of FLT3-ITD-driven leukemia and extend the survival of leukemic mice. Together, our work validates PRL2 as a novel druggable target for AML.

We previously found that loss of PRL2 does not change HSC number in the BM but decreases adult HSPC proliferation.[28] We now show that receptor tyrosine kinase, PI3K/AKT, and ERK signaling gene signatures are significantly downregulated in *Prl2* null fetal liver HSPCs. In addition, loss of Prl2 significantly decreased AKT, STAT5 and ERK phosphorylation in fetal liver cells. Given that fetal liver HSPCs are characterized by a massive expansion of HSCs whereas BM HSCs are much more quiescent, PRL2 effect could be associated with cell proliferation instead of "stem" ability in fetal livers.

Members of the CBL family E3 ubiquitin ligases share a highly conserved N-terminal tyrosine kinase-binding (TKB) domain, a short linker helical region (LHR), and a RING finger (RF) domain.[15] The LHR and RF domains dictate the E3 activity of CBL family members by serving as a structural platform for optimal binding of a ubiquitin-conjugating enzyme E2.[15] CBL's ubiquitination activity is stimulated by phosphorylation of a Tyr residue in a linker helix region (LHR).[39-41] Structural and biochemical studies show that phosphorylation of Tyr 371 activates CBL by inducing LHR conformational changes that eliminate autoinhibition and enable direct participation of LHR phosphotyrosine in the activation of E2~ubiquitin complex for catalysis.[41,47] This activation is required for receptor tyrosine kinase ubiquitination. We found that PRL2 associates with and dephosphorylates CBL in human leukemia cells

and that inhibition of PRL2 activity increases CBL Tyr 371 phosphorylation in human leukemia cells. Our results suggest that CBL/pTyr371 is a novel PRL2 substrate in leukemia cells.

Most *CBL* mutations in myeloid malignancies are found in the RING finger domain and the linker region of CBL.[19-21] Some CBL mutants such as CBL^{Y371H} and CBL-70Z do not have E3 ubiquitin ligase activity but compete against wild-type CBL and CBL-B, leading to prolonged activation of receptor tyrosine kinases after cytokine stimulation.[39, 40] Inactivating *CBL* mutations-mediated hematopoietic transformation in AML depends on FLT3 signaling.[48] Indeed, loss of CBL E3 ubiquitin ligase activity enhances the development of myeloid leukemia in FLT3-ITD mutant mice.[49] Further, myeloid leukemia development in CBL RING finger mutant mice is dependent on FLT3 signaling.[50] Our finding that PRL2 dephosphorylates CBL at Tyr 371 thereby compromising CBL's ability to ubiquitinate FLT3 is consistent with a tumor suppressor role for CBL in hematological malignancies. We previously showed that PRL2 is important for SCF/KIT signaling in HSPCs.[28] Thus, decreased AKT, ERK and STAT5 phosphorylation seen in *Prl2* null fetal HSPCs could be due to diminished FLT3 and KIT signaling. Given that CBL is the E3 ligase for both FLT3 and KIT,[15] it is possible that PRL2 could also promote KIT signaling in HSPCs through dephosphorylation of CBL at tyrosine 371.

Despite substantial efforts devoted to the development of FLT3 inhibitors, the effectiveness of these agents in AML has been limited.[6-8, 51] Even though FLT3 inhibitors show relative success at prolonging survival rates compared to the standards therapies, the short duration of response and therapeutic resistance are still a clinical challenge in AML treatment.[42, 51, 52] The strategies to overcome resistance mutations and provide durable remissions, such as a combination of inhibitors or use of more potent FLT3 inhibitors, have been evaluated.[9] Here we show that PRL2 functions upstream of FLT3 and promotes oncogenic FLT3 signaling in leukemia cells by inhibiting CBL mediated FLT3 ubiquitination

and degradation. We further demonstrate that PRL2 deletion or inhibition decrease leukemia burden and extends the survival of mice transplanted with human leukemia cells. Consequently, PRL2 inhibitors may offer an alternative strategy for AML treatment. To therapeutically target the PRL family members in cancer, we sought to exploit a unique regulatory property of the PRLs, namely their propensity for trimer formation, which is required for PRL-mediated cell growth and migration.[31, 36, 37, 53] Using structure-based virtual screening we identified compound 43 (PRLi), which disrupts PRL trimerization and blocks PRL induced cell proliferation and migration.[31] PRLi displays a respectable pharmacokinetic profile and exhibits not obvious toxicity to major tissues and organs in mice.[31] Notably, PRLi did not affect the viability of human cord blood mononuclear cells and $CD34^+$ cells.[27] PRLi treatment significantly reduced tumor volume in NSG mice transplanted with human melanoma cells.[31] Furthermore, we found that both human AML and acute lymphoblastic leukemia (ALL) cells are sensitive to PRLi treatment *in vitro*.[27,30] We now showed that *in vivo* PRLi treatment significantly reduces leukemia burden and extends the survival of NSG mice transplanted with primary human leukemia cells with FLT3-ITD mutations. Our ex vivo studies showed that FLT3 WT and FLT3 mutated primary AML samples are equally sensitive to PRL2 inhibition, suggesting that there is an underlying mechanism that is different among AML samples based on their mutations. PRL2 is highly expressed in some subtypes of AML[27] and AML patients with high *PRL2* expression have reduced overall survival compared to AML patients with low *PRL2* expression. It is possible that PRL2 utilizes distinct mechanisms to promote cell proliferation and enhance oncogenic signaling in different cellular context. We thus demonstrate that PRL2 is a novel druggable target in human AML.

Acknowledgements

Y. L. was supported by NIH R01 HL150624, R56 DK119524, R56 AG052501, DoD W81XWH-18-1-0265, DoD W81XWH-19-1-0575, the Leukemia &Lymphoma Society Translational Research Program award 6581-20 and the St. Baldrick's Foundation Scholar Award. Y.B. and Z.Y.Z. were supported by NIH R01 CA069202 and the Robert C. and Charlotte Anderson Chair Endowment. S. B. was supported

by a NIH F31 Award F31HL160120. H.C. was supported by Natural Science Foundation of Chongqing cstc2020jcyj-msxmX0969.

The authors would like to acknowledge the Flow Cytometry Core and In vivo Therapeutic Core Laboratories at the Indiana University, which were sponsored, in part, by the NIDDK Cooperative Center of Excellence in Hematology (CCEH) grant U54 DK106846.

Authorship

H.C., Y.B., M.K., Z.Y.Z., and Y.L. were responsible for the conception and/or design of the research. H.C., Y.B., M.K., S.X., W.C., S.B., S.C., J.M., F.N.M., S.V., J. P. R., J.W., Y.J., H.L., P.J., Z.Y.Z, and Y.L. were involved in acquisition, analysis or interpretation of data. J.M.C., H.S.B., L.S.L., J.K.A., E.A.E., W.T., H.B., D.T.H., and L.C.P. provided reagents and constructive advice to the study. H.C., Y.B., Z.Y.Z., and Y.L. wrote the manuscript. All authors read, comment on, and approved the manuscript.

Declaration of Interests

The authors declared no competing interests.

461 **References**

462 1. Roboz GJ. Treatment of acute myeloid leukemia in older patients. *Expert Review of Anticancer*
463 *Therapy*. 2007;7(3):285-295.
464 2. Roboz GJ. Current treatment of acute myeloid leukemia. *Current Opinion in Oncology*.
465 2012;24(6)
466 3. Burnett A, Wetzler M, Löwenberg B. Therapeutic Advances in Acute Myeloid Leukemia.
467 *Journal of Clinical Oncology*. 2011;29(5):487-494.
468 4. Toffalini F, Demoulin J-B. New insights into the mechanisms of hematopoietic cell
469 transformation by activated receptor tyrosine kinases. *Blood*. 2010;116(14):2429-2437.
470 5. Stirewalt DL, Meshinchi S. Receptor Tyrosine Kinase Alterations in AML – Biology and
471 Therapy. In: Nagarajan L, ed. *Acute Myelogenous Leukemia: Genetics, Biology and Therapy*. Springer
472 New York; 2010:85-108.
473 6. Kindler T, Lipka DB, Fischer T. FLT3 as a therapeutic target in AML: still challenging after all
474 these years. *Blood*. 2010;116(24):5089-5102.
475 7. Swords R, Freeman C, Giles F. Targeting the FMS-like tyrosine kinase 3 in acute myeloid
476 leukemia. *Leukemia*. 2012;26(10):2176-2185.
477 8. Metzelder S, Wang Y, Wollmer E, et al. Compassionate use of sorafenib in FLT3-ITD–positive
478 acute myeloid leukemia: sustained regression before and after allogeneic stem cell transplantation.
479 *Blood*. 2009;113(26):6567-6571.
480 9. Alfayez M, Kantarjian HM, Ravandi F, et al. Outcomes with Subsequent FLT3-Inhibitor
481 (FLT3i) Based Therapies in FLT3-Mutated (mu) Patients (pts) Refractory/Relapsed (R/R) to One or
482 More Prior FLT3 Inhibitor Based Therapies: A Single Center Experience. *Blood*. 2018;132:663.
483 10. Hope KJ, Jin L, Dick JE. Acute myeloid leukemia originates from a hierarchy of leukemic stem
484 cell classes that differ in self-renewal capacity. *Nature Immunology*. 2004;5:738-743.
485 11. Guzman ML, Jordan CT. Considerations for Targeting Malignant Stem Cells in Leukemia.
486 *Cancer Control*. 2004;11(2):97-104.

12. Kreso A, Dick JE. Evolution of the cancer stem cell model. *Cell Stem Cell*. 2014; 14: 275–91.

13. Gerber JM, Smith BD, Ngwang B, et al. A clinically relevant population of leukemic CD34(+)CD38(-) cells in acute myeloid leukemia. *Blood*. 2012; 119: 3571–7.

14. Garz AK, Wolf S, Grath S, et al. Azacitidine combined with the selective FLT3 kinase inhibitor crenolanib disrupts stromal protection and inhibits expansion of residual leukemia-initiating cells in *FLT3*-ITD AML with concurrent epigenetic mutations. *Oncotarget*. 2017;8(65):108738-108759.

15. Thien CBF, Langdon WY. Cbl: many adaptations to regulate protein tyrosine kinases. *Nature Reviews Molecular Cell Biology*. 2001;2(4):294-307.

16. Naramura M, Nandwani N, Gu H, Band V, Band H. Rapidly fatal myeloproliferative disorders in mice with deletion of Casitas B-cell lymphoma (Cbl) and Cbl-b in hematopoietic stem cells. *Proceedings of the National Academy of Sciences*. 2010;107(37):16274-16279.

17. An W, Nadeau SA, Mohapatra BC, et al. Loss of Cbl and Cbl-b ubiquitin ligases abrogates hematopoietic stem cell quiescence and sensitizes leukemic disease to chemotherapy. *Oncotarget*. 2015;6(12):10498-10509.

18. An W, Mohapatra BC, Zutshi N, et al. VAV1-Cre mediated hematopoietic deletion of CBL and CBL-B leads to JMML-like aggressive early-neonatal myeloproliferative disease. *Oncotarget*. 2016/09// 2016;7(37):59006-59016.

19. Makishima H, Cazzolli H, Szpurka H, et al. Mutations of e3 ubiquitin ligase cbl family members constitute a novel common pathogenic lesion in myeloid malignancies. *J Clin Oncol*. 2009;27(36):6109-6116.

20. Sanada M, Suzuki T, Shih L-Y, et al. Gain-of-function of mutated C-CBL tumour suppressor in myeloid neoplasms. *Nature*. 2009/08/01 2009;460(7257):904-908.

21. Niemeyer CM, Kang MW, Shin DH, et al. Germline CBL mutations cause developmental abnormalities and predispose to juvenile myelomonocytic leukemia. *Nat Genet*. 2010;42(9):794-800.

22. Nadeau SA, An W, Mohapatra BC, et al. Structural Determinants of the Gain-of-Function Phenotype of Human Leukemia-associated Mutant CBL Oncogene. *J Biol Chem*. 2017;292(9):3666-3682.

23. Bessette DC, Qiu D, Pallen CJ. PRL PTPs: mediators and markers of cancer progression. *Cancer and Metastasis Reviews*. 2008;27(2):231-252.

24. Ríos P, Li X, Köhn M. Molecular mechanisms of the PRL phosphatases. *The FEBS Journal*. 2013;280

25. Campbell AM, Zhang Z-Y. Phosphatase of regenerating liver: a novel target for cancer therapy. *Expert Opin Ther Targets*. 2014;18(5):555-569.

26. Kobayashi M, Chen S, Gao R, Bai Y, Zhang Z-Y, Liu Y. Phosphatase of regenerating liver in hematopoietic stem cells and hematological malignancies. *Cell Cycle*. 2014;13(18):2827-2835.

27. Kobayashi M, Chen S, Bai Y, et al. Phosphatase PRL2 promotes AML1-ETO-induced acute myeloid leukemia. *Leukemia*. 2017;31(6):1453-1457.

28. Kobayashi M, Bai Y, Dong Y, et al. PRL2/PTP4A2 phosphatase is important for hematopoietic stem cell self-renewal. *Stem Cells*. 2014;32(7):1956-1967.

29. Kobayashi M, Nabinger SC, Bai Y, et al. Protein Tyrosine Phosphatase PRL2 Mediates Notch and Kit Signals in Early T Cell Progenitors. *Stem Cells*. 2017;35(4):1053-1064.

30. Kobayashi M, Bai Y, Chen S, et al. Phosphatase PRL2 promotes oncogenic NOTCH1-Induced T-cell leukemia. *Leukemia*. 2017;31(3):751-754.

31. Bai Y, Yu Z-H, Liu S, et al. Novel Anticancer Agents Based on Targeting the Trimer Interface of the PRL Phosphatase. *Cancer Res*. 2016;76(16):4805-4815.

32. Lee BH, Tothova Z, Levine RL, et al. FLT3 mutations confer enhanced proliferation and survival properties to multipotent progenitors in a murine model of chronic myelomonocytic leukemia. *Cancer Cell*. 2007;12(4):367-380.

33. Dong Y, Zhang L, Zhang S, et al. Phosphatase of regenerating liver 2 (PRL2) is essential for placental development by down-regulating PTEN (Phosphatase and Tensin Homologue Deleted on Chromosome 10) and activating Akt protein. *J Biol Chem*. 2012;287(38):32172-32179.

34. Li Q, Bai Y, Lyle LT, et al. Mechanism of PRL2 phosphatase-mediated PTEN degradation and tumorigenesis. *Proceedings of the National Academy of Sciences*. 2020;117(34):20538-20548.

35. Borkin D, He S, Miao H, et al. Pharmacologic inhibition of the Menin-MLL interaction blocks progression of MLL leukemia in vivo. *Cancer Cell*. 2015;27(4):589-602.

36. Sun J-P, Wang W-Q, Yang H, et al. Structure and Biochemical Properties of PRL-1, a Phosphatase Implicated in Cell Growth, Differentiation, and Tumor Invasion. *Biochemistry*. 2005;44(36):12009-12021.

37. Sun J-P, Luo Y, Yu X, et al. Phosphatase Activity, Trimerization, and the C-terminal Polybasic Region Are All Required for PRL1-mediated Cell Growth and Migration*. *Journal of Biological Chemistry*. 2007;282(39):29043-29051.

38. Mercan F, Bennett AM. Analysis of protein tyrosine phosphatases and substrates. *Curr Protoc Mol Biol*. 2010;Chapter 18:Unit-18.16.

39. Dou H, Buetow L, Hock A, Sibbet GJ, Vousden KH, Huang DT. Structural basis for autoinhibition and phosphorylation-dependent activation of c-Cbl. *Nat Struct Mol Biol*. 2012;19(2):184-192.

40. Mohapatra B, Ahmad G, Nadeau S, et al. Protein tyrosine kinase regulation by ubiquitination: Critical roles of Cbl-family ubiquitin ligases. *Biochimica et Biophysica Acta (BBA) - Molecular Cell Research*. 2013;1833(1):122-139.

41. Ahmed SF, Buetow L, Gabrielsen M, et al. E3 ligase-inactivation rewires CBL interactome to elicit oncogenesis by hijacking RTK–CBL–CIN85 axis. *Oncogene*. 2021;40(12):2149-2164.

42. Lam SS, Martell JD, Kamer KJ, et al. Directed evolution of APEX2 for electron microscopy and proximity labeling. *Nat Methods*. 2015;12(1):51-54.

43. Lee S-Y, Kang M-G, Park J-S, Lee G, Ting Alice Y, Rhee H-W. APEX Fingerprinting Reveals the Subcellular Localization of Proteins of Interest. *Cell Reports*. 2016;15(8):1837-1847.

44. Tan B, Peng S, Yatim SMJM, Gunaratne J, Hunziker W, Ludwig A. An Optimized Protocol for Proximity Biotinylation in Confluent Epithelial Cell Cultures Using the Peroxidase APEX2. *STAR Protocols*. 2020;1(2):100074.

45. Tonks NK. Protein tyrosine phosphatases: from genes, to function, to disease. *Nature Reviews Molecular Cell Biology*. 2006;7(11):833-846.

46. Julien SG, Dubé N, Hardy S, Tremblay ML. Inside the human cancer tyrosine phosphatome. *Nature Reviews Cancer*. 2011;11(1):35-49.

47. Dou H, Buetow L, Sibbet GJ, Cameron K, Huang DT. Essentiality of a non-RING element in priming donor ubiquitin for catalysis by a monomeric E3. *Nat Struct Mol Biol*. 2013;20(8):982-986.

48. Sargin B, Choudhary C, Crosetto N, et al. Flt3-dependent transformation by inactivating c-Cbl mutations in AML. *Blood*. 2007;110(3):1004-1012.

49. Taylor SJ, Thien CBF, Dagger SA, et al. Loss of c-Cbl E3 ubiquitin ligase activity enhances the development of myeloid leukemia in FLT3-ITD mutant mice. *Experimental Hematology*. 2015;43(3):191-206.e1.

50. Rathinam C, Thien CBF, Flavell RA, Langdon WY. Myeloid Leukemia Development in c-Cbl RING Finger Mutant Mice Is Dependent on FLT3 Signaling. *Cancer Cell*. 2010/10/19/ 2010;18(4):341-352.

51. Kennedy VE, Smith CC. FLT3 Mutations in Acute Myeloid Leukemia: Key Concepts and Emerging Controversies. *Front Oncol*. 2020;10:612880-612880.

52. Lam SSY, Leung AYH. Overcoming Resistance to FLT3 Inhibitors in the Treatment of FLT3-Mutated AML. *Int J Mol Sci*. 2020;21(4):1537.

53. Bai Y, Luo Y, Liu S, et al. PRL-1 protein promotes ERK1/2 and RhoA protein activation through a non-canonical interaction with the Src homology 3 domain of p115 Rho GTPase-activating protein. *J Biol Chem*. 2011;286(49):42316-42324.

Figure Legends

Figure 1. FLT3 mutated AML patients with high *PRL2* expression have reduced overall survival

(A) Relative *PRL2* (*PTP4A2*) mRNA expression in AML patients with favorable or intermediated & poor cytogenetic risk.

(B) Relative *PRL2* (*PTP4A2*) mRNA expression in live or dead AML patients.

(C) Relative *PRL2* (*PTP4A2*) mRNA expression in AML patients with or without cytogenetic relapse.

(D) Overall survival of poor cytogenetic risk AML patients with high (n=17) or low (n=14) PRL2 expression.

(E) DEGs between the *PRL2* high expression group and *PRL2* low expression group in AML. Genes with P<0.05 and Log2FC >1 is indicated in red and blue colors in the volcano plot. Red indicates genes upregulated in the *PRL2* high expression group, whereas blue indicates genes downregulated in the *PRL2* high expression group. The X-axis is the log2-transformed fold change, and the Y-axis is the log10-transformed P-value.

(F) Gene Set Enrichment Analysis (GSEA) of gene transcription between the *PRL2* high expression group and *PRL2* low expression group in AML. Acute myeloid leukemia (AML), AML prognosis, leukemia stem cell, and hematopoietic stem cell gene signatures were enriched in the *PRL2* high expression group compared to the *PRL2* low expression group.

(G) GAEA showed that *FLT3*-mutated APL, FLT3 signaling, and cytokine-cytokine receptor interaction gene signatures are significantly enriched in the *PRL2* high expression group.

(H) GSEA showed that STAT5A targets, PI3K/AKT signaling pathway, and ERK1/ERK2/MAPK pathway gene signatures are significantly enriched in the *PRL2* high expression group.

(I) Relative *PRL2* (*PTP4A2*) mRNA expression in AML patients with or without *FLT3* mutation.

(J) Overall survival of *FLT3* mutation positive AML patients with high (n=20) or low (n=19) *PRL2* expression.

Figure 2. Prl2 deficiency alters gene transcription in murine hematopoietic stem and progenitor cells

(A) Heat map of Prl2-regulated genes that are upregulated (red) or downregulated (blue) ($Log_2FC < -1$, FDR<0.05, p<0.05) in *Prl2* null E14.5 (Embryonic day 14.5) fetal liver cells compared to WT fetal liver cells.

(B) GSEA analysis of gene transcription between WT and *Prl2* null E14.5 fetal liver cells. Hematopoiesis stem cell, receptor tyrosine kinases, PI3KAKT signaling pathway, and MAPK pathway gene signatures were significantly downregulated in *Prl2* null E14.5 fetal liver cells.

(C) GSEA showed that receptor regulator activity, receptor complex, cell surface, and receptor protein tyrosine kinase gene signatures were significantly downregulated in *Prl2* null E14.5 fetal liver cells.

(D) GSEA showed that regulation of receptor signaling pathway, positive regulation of ERK1 and ERK2 cascade, and positive regulation of MAPK cascade gene signatures were significantly downregulated in *Prl2* null E14.5 fetal liver cells.

(E) STRING protein-protein interaction network between downregulated genes ($Log_2FC >1$, FDR<0.5, p<0.05) related to FLT3 signaling in *Prl2* null E14.5 fetal liver cells.

(F) Quantitative RT-PCR analysis of gene expression in WT and *Prl2* null E14.5 fetal liver cells (n=4).

(G) Quantitative RT-PCR analysis of gene expression in WT and *Prl2* null bone marrow Lin^- cells (n=4).

(H) Immunoblot analysis of AKT, STAT5, and ERK phosphorylation in WT and *Prl2* null E14.5 fetal liver cells (n=3).

(I) Immunoblot analysis of AKT, STAT5, and ERK phosphorylation in WT and *Prl2* null bone marrow Lin^- cells (n=3).

Mean values (±SEM) are shown (*p<0.05, **p<0.01, and ***p<0.001).

Figure 3. Loss of Prl2 decreases the self-renewal capability of FLT3-ITD positive hematopoietic stem and progenitor cells.

(A–D) The frequency of LT-HSCs ($Lin^-Sca1^+cKit^+CD150^+CD48^-$), ST-HSCs ($Lin^-Sca1^+cKit^+CD150^-CD48^-$), MPPs ($Lin^-Sca1^+cKit^+CD150^-CD48^+$), and LSKs ($Lin^-Sca1^+cKit^+$) in the bone marrow (BM) of *Prl2*$^{+/+}$, *Prl2*$^{-/-}$, *Flt3*$^{+/ITD}$, *Flt3*$^{+/ITD}$*Prl2*$^{-/-}$, *Flt3*$^{ITD/ITD}$ and *Flt3*$^{ITD/ITD}$*Prl2*$^{-/-}$ mice (n=6 mice per group).

(E) Serial replating assays of *Prl2*$^{+/+}$, *Prl2*$^{-/-}$, *Flt3*$^{+/ITD}$, *Flt3*$^{+/ITD}$*Prl2*$^{-/-}$, *Flt3*$^{ITD/ITD}$ and *Flt3*$^{ITD/ITD}$*Prl2*$^{-/-}$ BM cells (n=3 independent experiments performed in triplicate).

(F) The percentage of donor-derived cells ($CD45.2^+$) in the peripheral blood (PB) of primary recipient mice (n = 9-10 mice per group).

(G-J) The frequency of LT-HSCs, ST-HSCs, MPPs and LSKs in the BM of primary recipient mice (n=6 mice per group).

(K) The percentage of donor-derived cells in PB of secondary recipient mice (n = 9-10 mice per group).

(L-O) The frequency of LT-HSCs, ST-HSCs, MPPs, and LSKs in the BM of secondary recipient mice (n=6 mice per group).

Mean values (±SEM) are shown (*p<0.05, **p<0.01, ***p < 0.001, ****p < 0.0001).

Figure 4. Prl2 is important for FLT3-ITD-induced myeloid proliferative neoplasm in mice.

(A) Loss of *Prl2* reduced splenomegaly seen in *Flt3*$^{+/ITD}$ and *Flt3*$^{ITD/ITD}$ mice.

(B) The spleen weights of *Prl2*$^{+/+}$, *Prl2*$^{-/-}$, *Flt3*$^{+/ITD}$, *Flt3*$^{+/ITD}$*Prl2*$^{-/-}$, *Flt3*$^{ITD/ITD}$ and *Flt3*$^{ITD/ITD}$*Prl2*$^{-/-}$ mice (n=6 mice per group).

(C) The frequency of LSKs in the spleen of *Prl2*$^{+/+}$, *Prl2*$^{-/-}$, *Flt3*$^{+/ITD}$, *Flt3*$^{+/ITD}$*Prl2*$^{-/-}$, *Flt3*$^{ITD/ITD}$ and *Flt3*$^{ITD/ITD}$*Prl2*$^{-/-}$ mice (n=6 mice per group).

(D) Kaplan-Meier survival curve of lethally irradiated recipient mice transplanted with $3x10^6$ *Prl2*$^{+/+}$, *Prl2*$^{-/-}$, *Flt3*$^{+/ITD}$, *Flt3*$^{+/ITD}$*Prl2*$^{-/-}$, *Flt3*$^{ITD/ITD}$ and *Flt3*$^{ITD/ITD}$*Prl2*$^{-/-}$ BM cells (n=9-10 mice per group).

(E-F) Red blood cell (RBC) and hemoglobin (HGB) counts in PB of recipient mice transplanted with *Prl2*$^{+/+}$, *Prl2*$^{-/-}$, *Flt3*$^{+/ITD}$, *Flt3*$^{+/ITD}$*Prl2*$^{-/-}$, *Flt3*$^{ITD/ITD}$ and *Flt3*$^{ITD/ITD}$*Prl2*$^{-/-}$ BM cells (n=9-10 mice per group).

(G) Representative flow cytometric analysis of myeloid cells (Gr1^{+}Mac1^{+}) and lymphocytes in PB of recipient mice repopulated with *Prl2*$^{+/+}$, *Prl2*$^{-/-}$, *Flt3*$^{+/ITD}$, *Flt3*$^{+/ITD}$*Prl2*$^{-/-}$, *Flt3*$^{ITD/ITD}$ and *Flt3*$^{ITD/ITD}$*Prl2*$^{-/-}$ BM cells.

(H) The frequency of myeloid cells (Gr1^{+}Mac1^{+}), B cells (B220^{+}) and T cells (CD3^{+}) in PB of recipient mice repopulated with *Prl2*$^{+/+}$, *Prl2*$^{-/-}$, *Flt3*$^{+/ITD}$, *Flt3*$^{+/ITD}$*Prl2*$^{-/-}$, *Flt3*$^{ITD/ITD}$ and *Flt3*$^{ITD/ITD}$*Prl2*$^{-/-}$ BM cells (n=8 mice per group).

(I) Representative H&E (10 x) images of the peripheral blood smears, bone marrow, spleen, and liver of recipient mice repopulated with *Flt3*$^{ITD/ITD}$ or *Flt3*$^{ITD/ITD}$*Prl2*$^{-/-}$ BM cells.

(J) The spleen weights of recipient mice repopulated with *Prl2*$^{+/+}$, *Prl2*$^{-/-}$, *Flt3*$^{+/ITD}$, *Flt3*$^{+/ITD}$*Prl2*$^{-/-}$, *Flt3*$^{ITD/ITD}$ and *Flt3*$^{ITD/ITD}$*Prl2*$^{-/-}$ BM cells (n=4 mice per group).

(K) Ectopic PRL2-CSDA expression decreased the proliferation of 32D cells expressing FLT3-ITD (n = 3).

(L) Expressing the PRL2-CSDA mutant, but not the WT PRL2, extended the survival of C3H/HeJ mice transplanted with 32D cells expressing FLT3-ITD (n= 7 mice per group).

Mean values (±SEM) are shown (*p<0.05, **p<0.01, ***p < 0.001, ****p < 0.0001).

Figure 5. Genetic and pharmacological inhibition of PRL2 decrease leukemia burden and extends the survival of mice transplanted with human leukemia cell lines

(A) Western blot analysis for PRL2 in MV-4-11 cells transduced with lentiviruses expressing a control shRNA (shCtrl) or PRL2 shRNAs (shPRL2 and shPRL2#2).

(B) Knocking down of PRL2 significantly decreased the colony formation of MV-4-11 cells (n=3). Representative images of the colonies are shown.

(C) Kaplan-Meier survival curve of sublethally irradiated NSG mice transplanted with $3x10^6$ MV-4-11 expressing shCtrl or shPRL2 (n=7 mice group).

(D) Flow cytometry quantification of GFP^+ cells in PB, BM, and spleen of NSG mice transplanted with MV-4-11 cells expressing control shRNA or shPRL2 (n=3 mice per group).

(E-F) The size and weight of spleen from NSG mice transplanted with MV-4-11 cells expressing control shRNA or shPRL2 (n=3 mice per group).

(G) PRL inhibitor (PRLi) treatment significantly decreased the colony formation ability in MV-4-11 (n=3). Representative images of the colonies are displayed.

(H) 3 x 10^6 MV-4-11 cells expressing luciferase were injected into sublethally irradiated NSG mice. One week after the transplantation, NSG mice were treated with DMSO or PRLi (25mg/kg, I.P.) daily for three weeks. The leukemia burden in NSG mice were monitored by In Vivo Image System (IVIS) once a week for three weeks (n=5 mice per group).

(I) Quantitative results from bioimaging (n=5 mice per group).

(J) Kaplan-Meier survival curve of NSG mice treated with DMSO or PRLi (n=7 mice per group).

(K) Flow cytometry analysis of human $CD45^+$ cells in PB, BM, and spleen of NSG mice transplanted with MV-4-11 cells after three weeks of DMSO or PRLi treatment (n=3 mice per group).

(L) PRLi treatment reduced splenomegaly seen in NSG mice transplanted with MV-4-11 cells.

(M) The spleen weights of NSG mice transplanted with MV-4-11 cells following three weeks of DMSO or PRLi treatment (n=3 mice per group).

Mean values (±SEM) are shown (*$p<0.05$, **$p<0.01$, ***$p < 0.001$, ****$p < 0.0001$).

Figure 6. Pharmacological inhibition of PRL2 reduces leukemia burden and extends the survival of mice transplanted with primary human AML cells

(A) PRLi treatment decreased the viability of primary human AML cells with FLT3-ITD mutation in a dosage-dependent manner.

(B) PRLi treatment reduced the colony forming ability of primary human AML cells with or without FLT3-ITD mutation. Samples 3153 and 3202 are from AML patients with WT FLT3, whereas samples 3142 and 3179 are from AML patients with FLT3-ITD.

(C) Cell cycle analysis of primary AML cells with FLT3-ITD mutation (AML3242) at 24 hours following DMSO or PRLi (10 μM) treatment.

(D) Apoptosis analysis of primary AML cells with FLT3-ITD (AML3242) at 24 hours following DMSO or PRLi (10 μM) treatment.

(E) Kaplan-Meier survival curve of NSG mice transplanted with 4 x 10^6 human $CD45^+$ leukemia cells (AML3179) following three weeks of DMSO or PRLi treatment (n=6 mice per group).

(F) Flow cytometry analysis of human $CD45^+$ cells in PB, BM, and spleen of NSG mice transplanted with 4 x 10^6 human $CD45^+$ leukemia cells (AML3179) after three weeks of DMSO or PRLi treatment (n=4 mice per group).

(G)Representative western blot analysis of AKT, STAT5 and ERK phosphorylation in $Prl2^{+/+}$, $Prl2^{-/-}$, $Flt3^{+/ITD}$, $Flt3^{+/ITD}Prl2^{-/-}$, $Flt3^{ITD/ITD}$ and $Flt3^{ITD/ITD}Prl2^{-/-}$ BM mononuclear cells.

(H) Representative western blot analysis of FLT3, AKT, STAT5 and ERK phosphorylation in MV-4-11 cells expressing shCtrl, shPRL2 or shPRL2#2 (Left) and following 24 hours of dimethyl sulfoxide (DMSO) or 5 μM PRLi treatment (Right).

(I) Representative western blot analysis of FLT3, AKT, STAT5, and ERK phosphorylation in primary AML cells with FLT3-ITD mutation (AML3080 and AML3220) following 24 hours of DMSO or PRLi (10 μM) treatment.

(J) Representative western blot analysis of AKT, STAT5 and ERK phosphorylation in human $CD45^+$ cells isolated from the BM of NSG mice at 4 weeks after transplantation with MV-4-11 cells expressing control shRNA or shPRL2 (Left panel, n=3 mice per group); human $CD45^+$ cells in the

BM of NSG mice transplanted with MV-4-11 cells following three weeks of DMSO or PRLi treatment (Right panel, n=3 mice per group).

(K) Representative western blot analysis of AKT, STAT5, and ERK phosphorylation in human $CD45^{+}$ cells isolated from the BM of NSG mice transplanted with PDX cells (AML3179) following three weeks of DMSO or PRLi treatment (n=3 mice per group).

Figure 7. PRL2 associates with and dephosphorylates CBL at tyrosine 371 in leukemia cells

(A) Genetic knock down PRL2 decreased FLT3 half-life in MV-4-11 cells.

(B) Genetic knock down PRL2 enhanced FLT3 ubiquitination in MV-4-11 cells.

(C) Total cellular proteins from MV-4-11 cells were isolated, incubated with GST, GST-PRL2 or GST-PRL2-CSDA and immunoblotted with antibody against FLT3, CBL, SHP2, and PLC-γ.

(D) Co-immunoprecipitation assays showed that PRL2 interacts with FLT3 and CBL in MV-4-11 cells.

(E) Immunofluorescence analysis showed that PRL2 co-localizes with CBL in MV-4-11 cells.

(F) Representative western blot analysis showed that ectopic PRL2 expression decreases tyrosine phosphorylation of CBL in 293 cells.

(G) Representative western blot analysis showed that knocking down of PRL2 increases the tyrosine phosphorylation of CBL in MV-4-11 cells.

(H) Representative western blot analysis showed that knocking down of PRL2 increases CBL phosphorylation at tyrosine 371 in MV-4-11 cells.

(I) Representative western blot analysis showed that ectopic expression of PRL2-CSDA increases CBL phosphorylation at tyrosine 371 in MV-4-11 cells.

(J) APEX2-PRL2 proximity labeling was performed in HA-CBL or HA-Cbl^{Y371F} transiently expressed 293 cells stably expressing APEX2-PRL2. After labeling, biotinylated proteins are enriched with neutravidin beads and examined with anti-HA and anti-PRL2 antibodies by Western blot analysis.

(K-L) PRL2-CSDA substrate trapping assays was performed in HA-CBL or HA- Cbl^{Y371F} transiently expressed HeLa (J) or 293 (K) cells stably expressing Flag-PRL2-CSDA. After Anti-Flag pulldown, bound proteins were boiled in 50 μL Laemmli sample buffer and examined with anti-HA, anti-PRL2 antibodies by Western blot analysis.

Figure 1

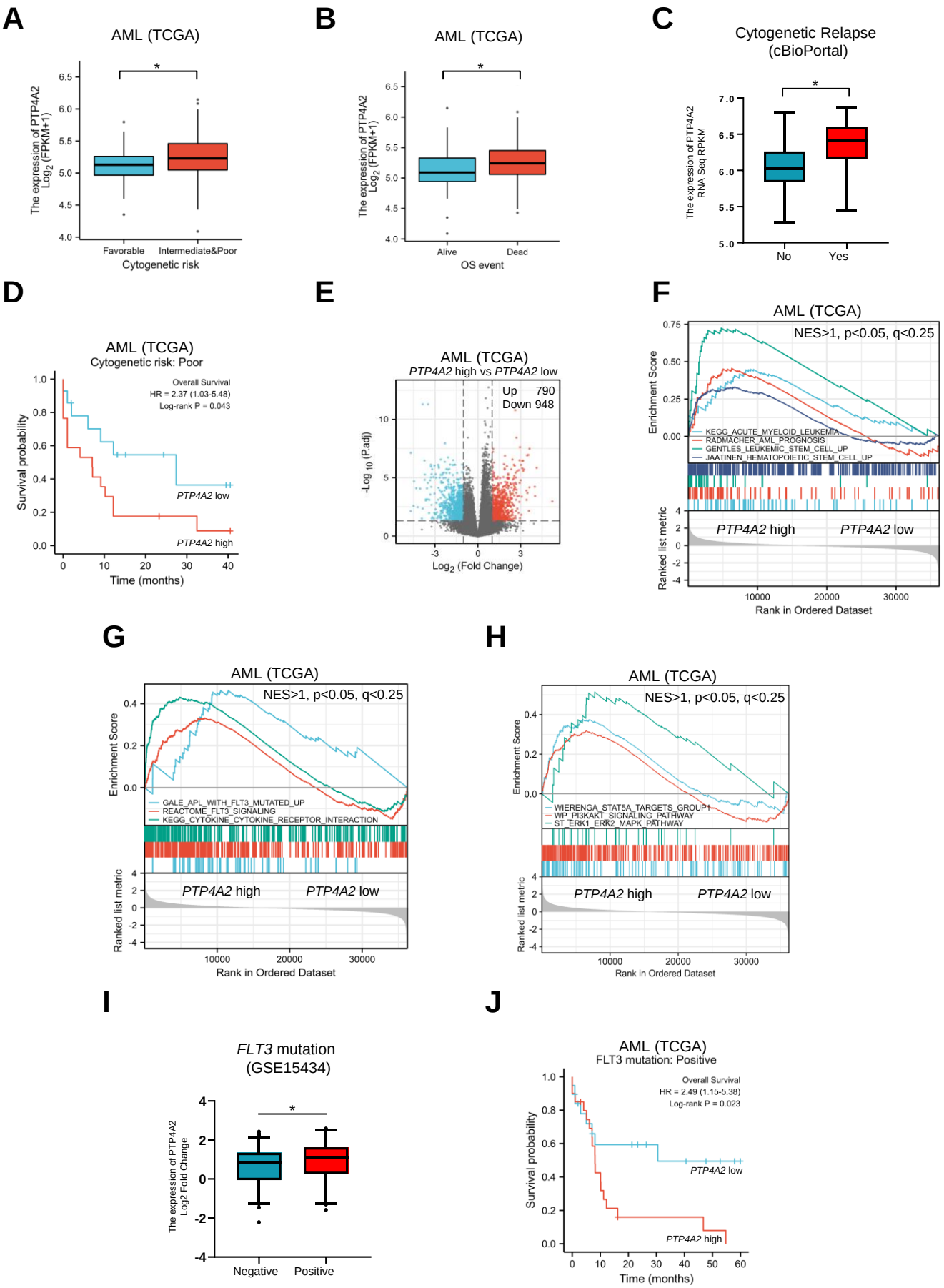
A
AML (TCGA)
The expression of PTP4A2 Log2 (FPKM+1)
Favorable
Intermediate&Poor
Cytogenetic risk
B
AML (TCGA)
The expression of PTP4A2 Log2 (FPKM+1)
Alive
Dead
OS event
C
Cytogenetic Relapse (cBioPortal)
The expression of PTP4A2 RNA Seq RPKM
No
Yes
D
AML (TCGA)
Cytogenetic risk: Poor
Overall Survival
HR = 2.37 (1.03-5.48)
Log-rank P = 0.043
PTP4A2 low
PTP4A2 high
Survival probability
Time (months)
E
AML (TCGA)
PTP4A2 high vs PTP4A2 low
Up 790
Down 948
-Log 10 (P.adj)
Log2 (Fold Change)
F
AML (TCGA)
NES>1, p<0.05, q<0.25
Enrichment Score
KEGG_ACUTE_MYELOID_LEUKEMIA
RADMACHER_AML_PROGNOSIS
GENTLES_LEUKEMIC_STEM_CELL_UP
JAATINEN_HEMATOPOIETIC_STEM_CELL_UP
PTP4A2 high
PTP4A2 low
Ranked list metric
Rank in Ordered Dataset
G
AML (TCGA)
NES>1, p<0.05, q<0.25
Enrichment Score
GALE_APL_WITH_FLT3_MUTATED_UP
REACTOME_FLT3_SIGNALING
KEGG_CYTOKINE_CYTOKINE_RECEPTOR_INTERACTION
PTP4A2 high
PTP4A2 low
Ranked list metric
Rank in Ordered Dataset
H
AML (TCGA)
NES>1, p<0.05, q<0.25
Enrichment Score
WIERENGA_STAT5A_TARGETS_GROUP1
WP_PI3KAKT_SIGNALING_PATHWAY
ST_ERK1_ERK2_MAPK_PATHWAY
PTP4A2 high
PTP4A2 low
Ranked list metric
Rank in Ordered Dataset
I
FLT3 mutation (GSE15434)
The expression of PTP4A2 Log2 Fold Change
Negative
Positive
J
AML (TCGA)
FLT3 mutation: Positive
Overall Survival
HR = 2.49 (1.15-5.38)
Log-rank P = 0.023
PTP4A2 low
PTP4A2 high
Survival probability
Time (months)

Figure 2

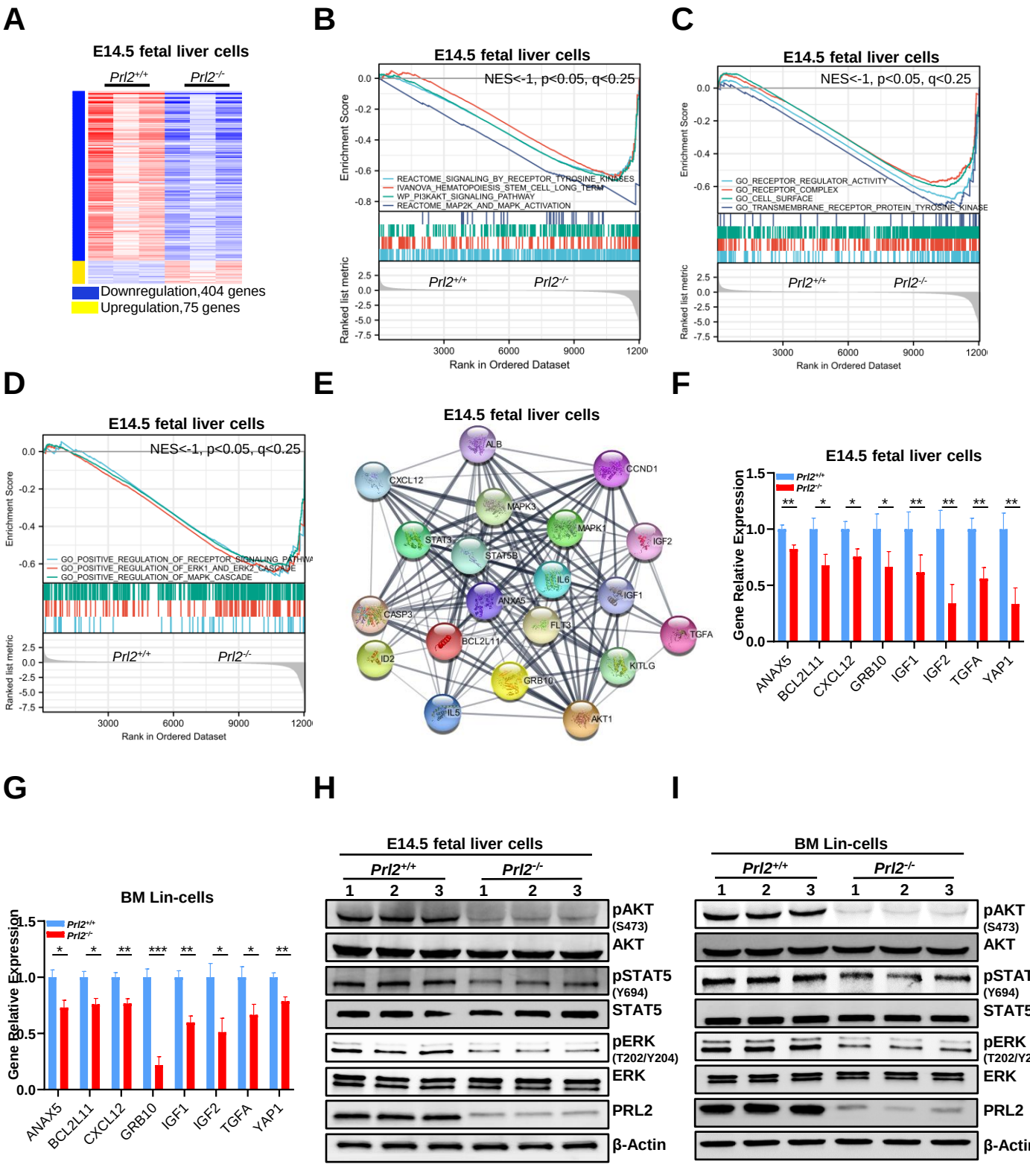
A
E14.5 fetal liver cells
Prl2+/+
Prl2-/-
Downregulation,404 genes
Upregulation,75 genes
B
E14.5 fetal liver cells
NES<-1, p<0.05, q<0.25
Enrichment Score
REACTOME_SIGNALING_BY_RECEPTOR_TYROSINE_KINASES
IVANOVA_HEMATOPOIESIS_STEM_CELL_LONG_TERM
WP_PI3KAKT_SIGNALING_PATHWAY
REACTOME_MAP2K_AND_MAPK_ACTIVATION
Ranked list metric
Prl2+/+
Prl2-/-
Rank in Ordered Dataset
C
E14.5 fetal liver cells
NES<-1, p<0.05, q<0.25
Enrichment Score
GO_RECEPTOR_REGULATOR_ACTIVITY
GO_RECEPTOR_COMPLEX
GO_CELL_SURFACE
GO_TRANSMEMBRANE_RECEPTOR_PROTEIN_TYROSINE_KINASE
Ranked list metric
Prl2+/+
Prl2-/-
Rank in Ordered Dataset
D
E14.5 fetal liver cells
NES<-1, p<0.05, q<0.25
Enrichment Score
GO_POSITIVE_REGULATION_OF_RECEPTOR_SIGNALING_PATHWA
GO_POSITIVE_REGULATION_OF_ERK1_AND_ERK2_CASCADE
GO_POSITIVE_REGULATION_OF_MAPK_CASCADE
Ranked list metric
Prl2+/+
Prl2-/-
Rank in Ordered Dataset
E
E14.5 fetal liver cells
ALB
CCND1
CXCL12
MAPK3
MAPK1
IGF2
STAT3
STAT5B
IL6
IGF1
ANXA5
CASP3
FLT3
TGFA
BCL2L11
ID2
KITLG
GRB10
IL5
AKT1
F
E14.5 fetal liver cells
Prl2+/+
Prl2-/-
Gene Relative Expression
ANAX5
BCL2L11
CXCL12
GRB10
IGF1
IGF2
TGFA
YAP1
G
BM Lin-cells
Prl2+/+
Prl2-/-
Gene Relative Expression
ANAX5
BCL2L11
CXCL12
GRB10
IGF1
IGF2
TGFA
YAP1
H
E14.5 fetal liver cells
Prl2+/+
Prl2-/-
1 2 3 1 2 3
pAKT (S473)
AKT
pSTAT5 (Y694)
STAT5
pERK (T202/Y204)
ERK
PRL2
β-Actin
I
BM Lin-cells
Prl2+/+
Prl2-/-
1 2 3 1 2 3
pAKT (S473)
AKT
pSTAT5 (Y694)
STAT5
pERK (T202/Y204)
ERK
PRL2
β-Actin

Figure 3

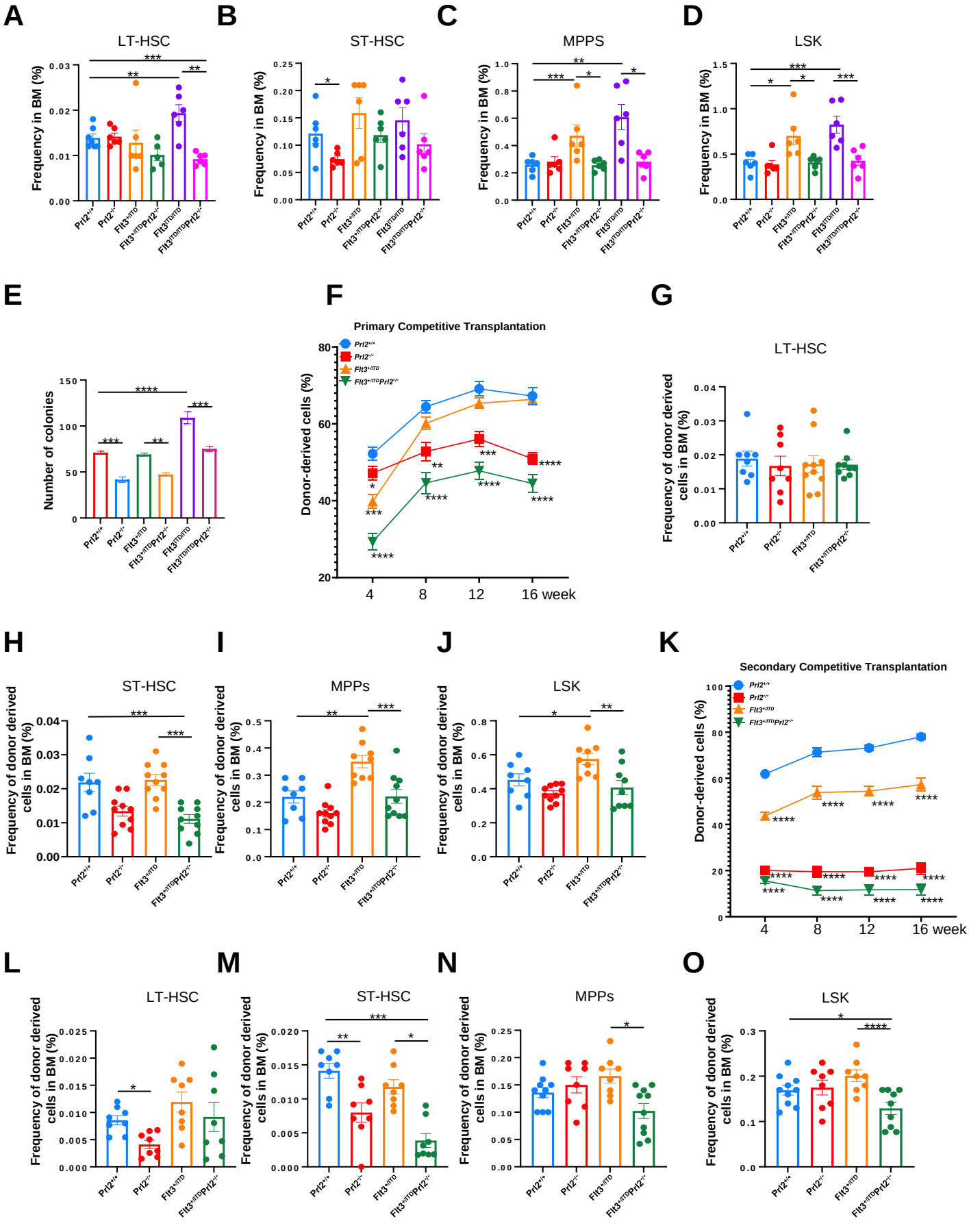
A
LT-HSC
Frequency in BM (%)
B
ST-HSC
Frequency in BM (%)
C
MPPS
Frequency in BM (%)
D
LSK
Frequency in BM (%)
Prl2+/+
Prl2-/-
Flt3+/ITD
Flt3+/ITDPrl2-/-
Flt3ITD/ITD
Flt3ITD/ITDPrl2-/-
E
Number of colonies
F
Primary Competitive Transplantation
Donor-derived cells (%)
4
8
12
16 week
G
LT-HSC
Frequency of donor derived cells in BM (%)
H
ST-HSC
Frequency of donor derived cells in BM (%)
I
MPPs
Frequency of donor derived cells in BM (%)
J
LSK
Frequency of donor derived cells in BM (%)
K
Secondary Competitive Transplantation
Donor-derived cells (%)
4
8
12
16 week
L
LT-HSC
Frequency of donor derived cells in BM (%)
M
ST-HSC
Frequency of donor derived cells in BM (%)
N
MPPs
Frequency of donor derived cells in BM (%)
O
LSK
Frequency of donor derived cells in BM (%)

Figure 4

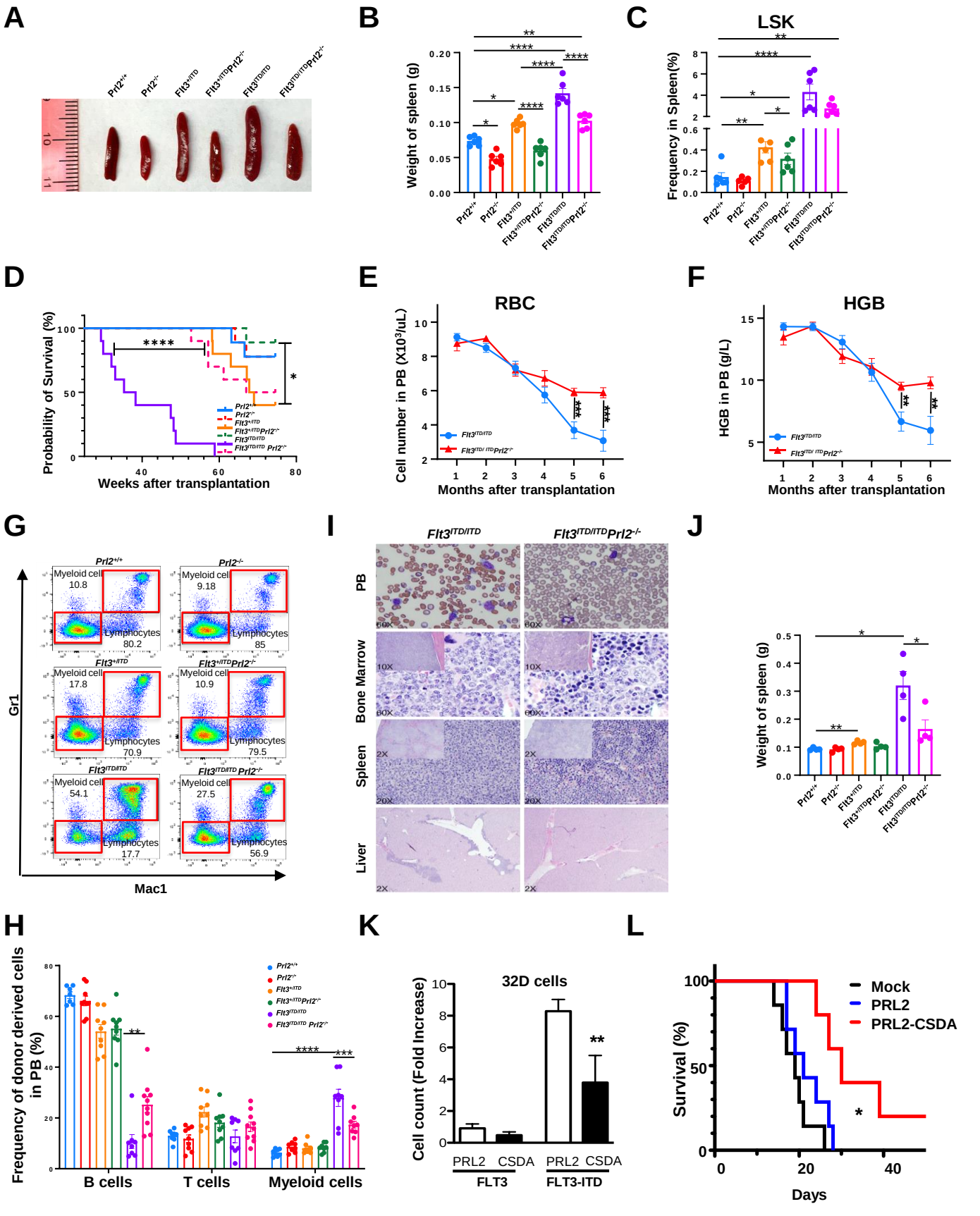
A
B
C
LSK
Weight of spleen (g)
Frequency in Spleen(%)
D
Probability of Survival (%)
Weeks after transplantation
E
RBC
Cell number in PB (X10³/uL)
Months after transplantation
F
HGB
HGB in PB (g/L)
Months after transplantation
G
Myeloid cell
Lymphocytes
Gr1
Mac1
I
PB
Bone Marrow
Spleen
Liver
J
Weight of spleen (g)
H
Frequency of donor derived cells in PB (%)
B cells
T cells
Myeloid cells
K
32D cells
Cell count (Fold Increase)
PRL2
CSDA
FLT3
FLT3-ITD
L
Survival (%)
Days
Mock
PRL2
PRL2-CSDA

Figure 5

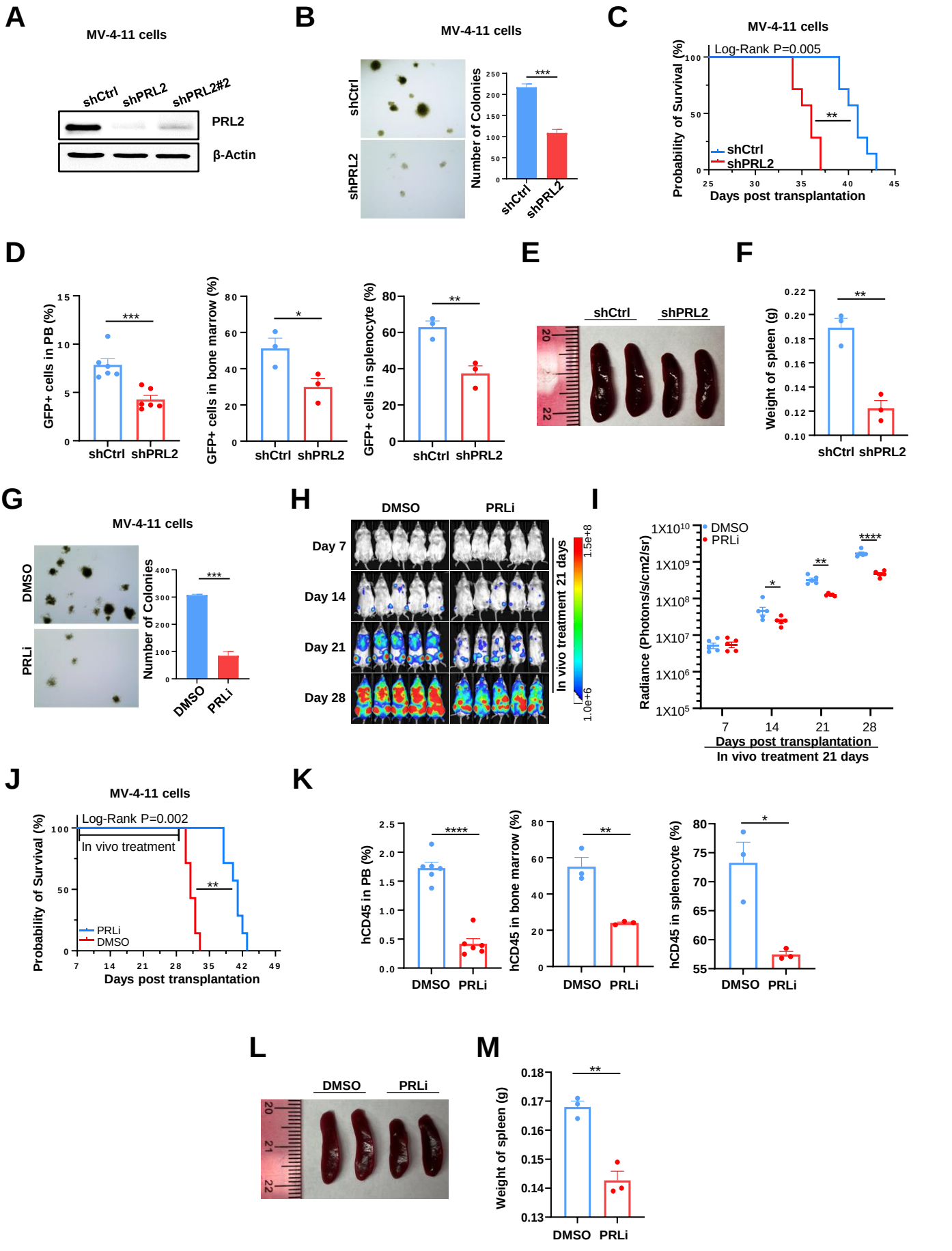
A
MV-4-11 cells
shCtrl
shPRL2
shPRL2#2
PRL2
β-Actin
B
MV-4-11 cells
shCtrl
shPRL2
Number of Colonies
***
C
MV-4-11 cells
Log-Rank P=0.005
Probability of Survival (%)
shCtrl
shPRL2
**
Days post transplantation
D
GFP+ cells in PB (%)
***
GFP+ cells in bone marrow (%)
*
GFP+ cells in splenocyte (%)
**
shCtrl
shPRL2
E
shCtrl
shPRL2
F
Weight of spleen (g)
**
shCtrl
shPRL2
G
MV-4-11 cells
DMSO
PRLi
Number of Colonies
***
H
DMSO
PRLi
Day 7
Day 14
Day 21
Day 28
In vivo treatment 21 days
1.5e+8
1.0e+6
I
DMSO
PRLi
Radiance (Photons/s/cm2/sr)
*
**
****
Days post transplantation
In vivo treatment 21 days
J
MV-4-11 cells
Log-Rank P=0.002
In vivo treatment
Probability of Survival (%)
**
PRLi
DMSO
Days post transplantation
K
hCD45 in PB (%)
****
hCD45 in bone marrow (%)
**
hCD45 in splenocyte (%)
*
DMSO
PRLi
L
DMSO
PRLi
M
Weight of spleen (g)
**
DMSO
PRLi

Figure 6

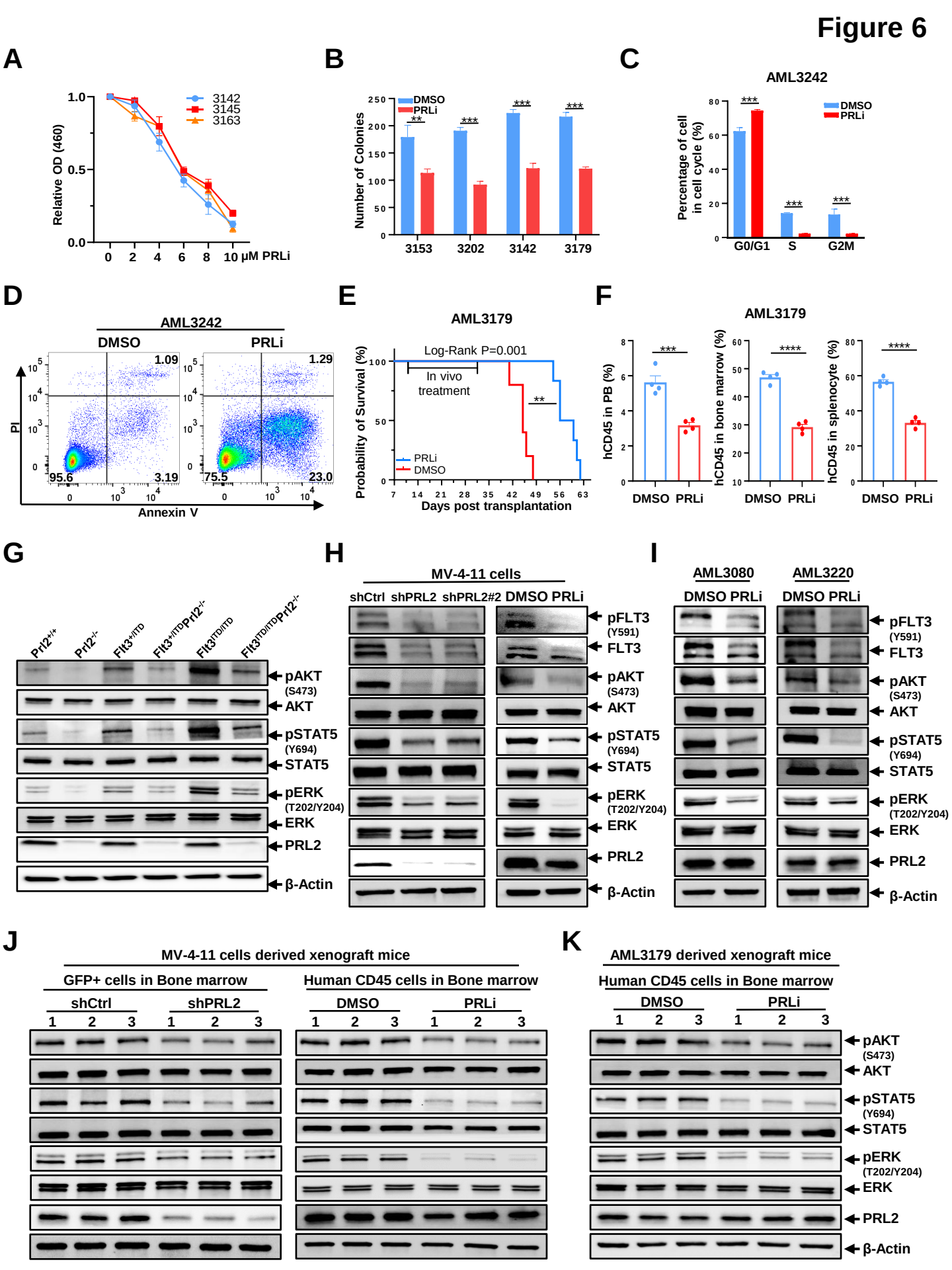
A
Relative OD (460)
3142
3145
3163
μM PRLi
B
Number of Colonies
DMSO
PRLi
3153
3202
3142
3179
C
AML3242
Percentage of cell in cell cycle (%)
DMSO
PRLi
G0/G1
S
G2M
D
AML3242
DMSO
PRLi
PI
Annexin V
95.6
3.19
75.5
23.0
E
AML3179
Log-Rank P=0.001
In vivo treatment
Probability of Survival (%)
Days post transplantation
F
AML3179
hCD45 in PB (%)
hCD45 in bone marrow (%)
hCD45 in splenocyte (%)
DMSO
PRLi
G
pAKT (S473)
AKT
pSTAT5 (Y694)
STAT5
pERK (T202/Y204)
ERK
PRL2
β-Actin
H
MV-4-11 cells
shCtrl
shPRL2
shPRL2#2
DMSO
PRLi
pFLT3 (Y591)
FLT3
I
AML3080
AML3220
J
MV-4-11 cells derived xenograft mice
GFP+ cells in Bone marrow
Human CD45 cells in Bone marrow
shCtrl
shPRL2
K
AML3179 derived xenograft mice
Human CD45 cells in Bone marrow

Figure 7

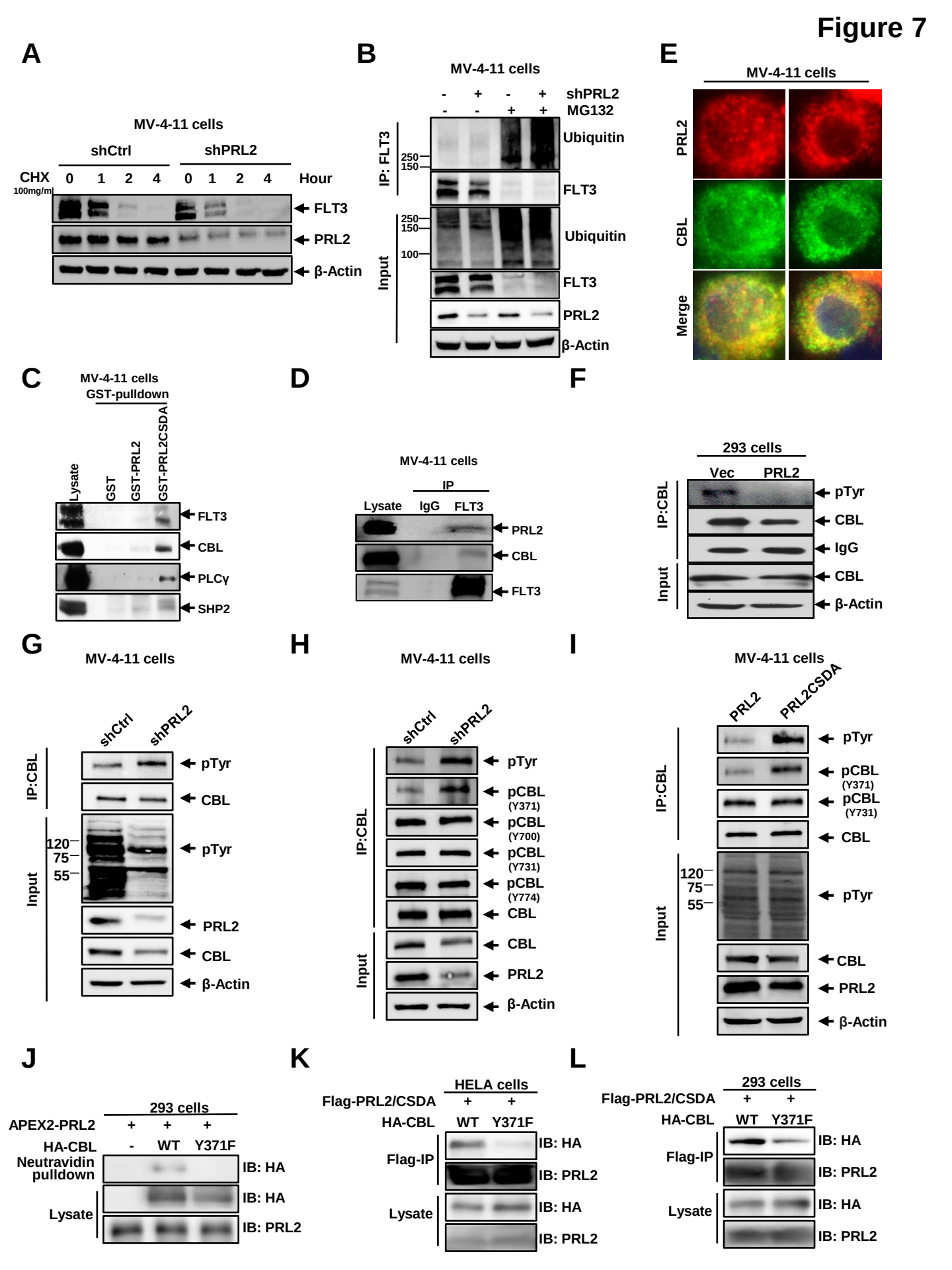
A
MV-4-11 cells
shCtrl
shPRL2
CHX 100mg/ml
0 1 2 4 0 1 2 4 Hour
FLT3
PRL2
β-Actin
B
MV-4-11 cells
shPRL2
MG132
IP: FLT3
Ubiquitin
FLT3
Input
Ubiquitin
FLT3
PRL2
β-Actin
250
150
100
E
MV-4-11 cells
PRL2
CBL
Merge
C
MV-4-11 cells
GST-pulldown
Lysate
GST
GST-PRL2
GST-PRL2CSDA
FLT3
CBL
PLCγ
SHP2
D
MV-4-11 cells
IP
Lysate
IgG
FLT3
PRL2
CBL
FLT3
F
293 cells
Vec
PRL2
IP:CBL
Input
pTyr
CBL
IgG
CBL
β-Actin
G
MV-4-11 cells
shCtrl
shPRL2
IP:CBL
Input
pTyr
CBL
pTyr
PRL2
CBL
β-Actin
120
75
55
H
MV-4-11 cells
shCtrl
shPRL2
IP:CBL
Input
pTyr
pCBL (Y371)
pCBL (Y700)
pCBL (Y731)
pCBL (Y774)
CBL
CBL
PRL2
β-Actin
I
MV-4-11 cells
PRL2
PRL2CSDA
IP:CBL
Input
pTyr
pCBL (Y371)
pCBL (Y731)
CBL
pTyr
CBL
PRL2
β-Actin
120
75
55
J
293 cells
APEX2-PRL2
HA-CBL
-
WT
Y371F
Neutravidin pulldown
Lysate
IB: HA
IB: HA
IB: PRL2
K
HELA cells
Flag-PRL2/CSDA
HA-CBL
WT
Y371F
Flag-IP
Lysate
IB: HA
IB: PRL2
IB: HA
IB: PRL2
L
293 cells
Flag-PRL2/CSDA
HA-CBL
WT
Y371F
Flag-IP
Lysate
IB: HA
IB: PRL2
IB: HA
IB: PRL2

PRL2 phosphatase enhances oncogenic FLT3 signaling via dephosphorylation of the E3 ubiquitin ligase CBL at tyrosine 371

Supplementary Information

Supplementary materials and methods

Human AML cell lines

Human AML cell lines, including MV-4-11, MOLM-13, K562, and U937, were obtained from ATCC (List in supplemental Table 2). All cell lines were authenticated by SRT profiling and tested for mycoplasma contamination.

Patient samples

AML samples were collected by Dr. H. Scott Boswell after informed consent. Mononuclear blasts from each sample were isolated by Ficoll (Axis-Shield) density centrifugation, and Trypan Blue Exclusion Assay was used to detect the cell viability. Protocols for sample handling and data analysis were approved by Indiana University Cancer center and Roudebush VA Medical Center Ethics Committee and were performed in compliance with the Declaration of Helsinki. Patient information is shown in supplemental Table 1.

Flow cytometry

Murine hematopoietic stem and progenitor cells were identified and evaluated by flow cytometry using a single cell suspension of bone marrow mononuclear cells (BMMCs). Hematopoietic stem and progenitors are purified based upon the expression of surface markers. BM cells were obtained from tibia, femur and iliac crest (6 from each mouse) by flushing cells out of the bone using a syringe and phosphate-buffered saline (PBS) with 2mM EDTA. Red blood cells (RBCs) were lysed by RBC lysis buffer (eBioscience) prior to staining. We defined hematopoietic stem and progenitor as well mature cells by flow cytometry markers. LT-HSCs ($Lin^-Sca1^+cKit^+CD150^+CD48^-$), ST-HSCs ($Lin^-Sca1^+cKit^+CD150^-CD48^-$), MPPs ($Lin^-Sca1^+cKit^+CD150^-CD48^+$), LSKs ($Lin^-Sca1^+cKit^+$), MyePro ($Lin^-Sca1^-cKit^+$), MEP ($Lin^-Sca1^-cKit^+CD34^-CD16/32^-$), CMP ($Lin^-Sca1^-cKit^+CD34^+CD16/32^-$), and GMP ($Lin^-Sca1^-cKit^+CD34^+CD16/32^+$), myeloid cells ($Gr1^+Mac1^+$), B cells ($B220^+$) and T cells ($CD3^+$). Experiments

were performed on FACS LSR IV cytometers (BD Biosciences) and analyzed by using the FlowJo_v10 software (TreeStar). All antibodies were listed in Supplementary table 2.

Transplantation assays

For competitive bone marrow transplantation assays, 5 x 10^5 BM cells ($CD45.2^+$) isolated from *Prl2*$^{+/+}$, *Prl2*$^{-/-}$, *Flt3*$^{+/ITD}$, and *Flt3*$^{+/ITD}$*Prl2*$^{-/-}$ mice together with 5 x 10^5 competitor BM cells ($CD45.1^+$) were injected into lethally irradiated (9.5 Gy) B6.SJL mice ($CD45.1^+$) via tail vein. At 16 weeks following primary transplantation, 3 x 10^6 BM cells isolated from primary recipients were transplanted into lethally irradiated secondary recipient mice ($CD45.1^+$). The engraftment of donor cells in peripheral blood and bone marrow were determined by flow cytometry analysis.

To determine the impact of PRL2 deficiency on FLT3-ITD-induced MPN, 3 x 10^6 bone marrow cells isolated from *Prl2*$^{+/+}$, *Prl2*$^{-/-}$, *Flt3*$^{+/ITD}$, *Flt3*$^{+/ITD}$*Prl2*$^{-/-}$, *Flt3*$^{ITD/ITD}$ and *Flt3*$^{ITD/ITD}$*Prl2*$^{-/-}$ mice were transplanted into lethally irradiated B6.SJL mice via tail vein.

To determine the impact of PRL2 deficiency on human leukemia cells *in vivo*, 3 x 10^6 transduced MV-4-11 or MOLM-13 cells (GFP^+) were injected into sublethally irradiated (2.5 Gy) NSG mice via tail vein.

To determine the efficacy of PRLi on primary human leukemia cells *in vivo*, we generated two patient-derived xenograft (PDX) models of AML in NSGS mice. 1 x 10^6 primary AML mononuclear cells with FLT3-ITD mutation were injected into sublethally irradiated (2.5 Gy) NSGS mice via tail vein to expand primary human AML cells *in vivo*. 12 to 16 weeks post primary transplantation, we confirmed the engraftment of human $CD45^+$ ($huCD45^+$) AML in NSGS mice and utilized the human $CD45^+$ cell enrichment kit to isolate human cells from the bone marrow of NSGS mice. We transplanted 4 x 10^6 human $CD45^+$ leukemia cells isolated from the BM of primary recipients into sublethally irradiated (2.5 Gy) NSG mice via tail vein injection. After confirmation of human leukemia engraftment in peripheral

blood of NSG mice (>1% human $CD45^+$ cells), NSG mice were treated with vehicle (10% DMSO) or PRLi (25 mg/kg, I.P.) daily for three weeks.

PRLi treatment *in vivo*

After confirmed the human cell engraftment by checking the human $CD45^+$ cells in peripheral blood reach to 1% by flow, the NSG mice start to receive the PRLi treatment. The small molecule inhibitor of PRL (PRLi, compound 43) was synthesized as described previously.[31] PRLi were dissolved in DMSO at 25mg/ml stocking concentration saved in -80°C freezer. PRLi stock solution or DMSO was diluted in PBS before administration. 25mg/kg PRLi or DMSO was administrated by intraperitoneal injection for consecutive 21 days.

Immunoblotting analysis

Cells were washed with ice-cold PBS and lysed on ice for 30 min in lysis buffer (50 mM Tris-HCl, pH 7.4, 150 mM NaCl, 1% Triton X-100, and 10% glycerol) supplemented with a Complete Protease Inhibitor tablet (Roche Applied Science). Cell lysates were cleared by centrifugation at 15,000 rpm for 10 min. The lysate protein concentration was estimated using a BCA protein assay kit (Pierce). The protein samples were boiled with sample buffer, separated by SDS-PAGE, transferred electrophoretically to a nitrocellulose membrane, and immunoblotted with appropriate antibodies, followed by incubation with horseradish peroxidase-conjugated secondary antibodies. The blots were developed by the enhanced chemiluminescence technique (ECL kit, GE Healthcare). Representative results from at least two independent experiments are shown. Representative results from at least two independent experiments are shown. All antibodies were listed in Supplementary table 2.

***In vivo* image system**

Bioimaging of leukemia burden *in vivo* was performed by Spectral Lago System at Northwestern University Center for Advanced Microscopy generously supported by NCI CCSG P30 CA060553

awarded to the Robert H Lurie Comprehensive Cancer Center. Before imaging, Luciferin (in vivo grade, Gold Bio, CAS# 115144-35-9) was prepared in PBS, and 150 mg/kg Luciferin was injected by i.p., after 10 minutes. The signal data was analyzed by the Aura software.

Production of Retrovirus and Lentivirus

Retroviral particles were produced by transfection of Phoenix E cells with MSCV-IRES-GFP, MSCV-PRL2-IRES-GFP, MSCV-PRL2-CSDA-IRES-GFP, MSCV-FLT3-IRES-GFP, or MSCV-FLT3-ITD-IRES-GFP plasmids, according to standard protocols. Mouse hematopoietic progenitor cells were transduced on retronectin (Takara)-coated non-tissue culture plates with high-titer retroviral suspensions. Twenty-four hours after infection, GFP-positive cells were sorted by FACS. Transduced cells were then transplanted into lethally irradiated recipient mice. The presence of GFP^+ cells in the peripheral blood was measured by flow cytometry analysis.

Lentiviral shLuciferase was a gift from Huipin Liu laboratory at the Northwestern University. Lentiviral shRNA plasmid (pLB) was purchased from Addgene (11619). Oligonuculeotides targeting control (Luciferase) and human PRL2 cDNAs were cloned into the pLB plasmid. Oligonuculeotide sequences are available upon request. Lentiviral particles were generated by standard method using the third-generation packaging system (pMDL, pMD2.G, and pRSV-Rev). Human AML cell lines were infected with high-titer lentiviral suspensions. 48 hours after infection, GFP-positive cells were sorted by FACS. The reduction of PRL2 proteins was determined by immunoblot analysis.

Colony formation unit assays

The colony formation of murine bone marrow Lin^- cells was determined in methylcellulose medium (MethoCult GF M3434, StemCell Technologies). Bone marrow Lin^- cells were isolated by mouse Lin- cell depletion kit. Lin^- cells were transduced with MIGR1 (MSCV-IRES-GFP), MIGR1-FLT3 (MSCV-

FLT3-IRES-GFP), or MIGR1-FLT3-ITD (MSCV-FLT3-ITD-IRES-GFP) retrovirus. 48 hours after infection, GFP positive cells were sorted by FACS. 5 x 10^3 GFP^+ cells were seed into methylcellulose medium (6-well plate). Colonies were scored after 7 days of the initial culture.

The colony formation of mice bone marrow cells was determined in methylcellulose medium (MethoCult GF M3434, StemCell Technologies) using 2 x 10^4 BM cells per well (6-well plate). Colonies were scored after 7 days of the initial culture.

The colony formation of human leukemia cells was determined in methylcellulose medium (MethoCult H4435, StemCell Technologies) using 1 x 10^3 leukemia cells or 5 x 10^4 primary AML patient BM cells per well (6-well plate). Colonies were scored after 10 days of culture.

Proliferation assays

Bone marrow Lin^- cells were transduced with MIGR1 (MSCV-IRES-GFP), MIGR1-FLT3 (MSCV-FLT3-IRES-GFP), or MIGR1-FLT3-ITD (MSCV-FLT3-ITD-IRES-GFP) retrovirus. 48 hours after infection, GFP positive cells were sorted by FACS. 2 x 10^6 GFP^+ cells were cultured in serum-free medium with or without 100ng/ml human FLT3 ligand for 48 hours.

For proliferation assay using primary AML patient samples, 1 x 10^5 cells were treated with or without gradient concentration of PRLi in 96 well plate. After 24 hours, 10 μl of WST-1 added to each well and incubate at 37° C for 2 hours. Experiments were performed on SpectraMax iD3.

To determine the specificity of PRLi on PRL2 in leukemia cells, MV-4-11 and MOLM-13 cells were transduced with retroviruses expressing GFP (MSCV-IRES-GFP), PRL2 (MSCV-PRL2-IRES-GFP), or PRL2-CSDA (MSCV- PRL2-CSDA -IRES-GFP). GFP positive cells were sorted by FACS. 2 x 10^6 GFP^+ cells were cultured with or without 5 μM PRLi for 7 days and cell viability was determined by Trypan blue staining.

Cell cycle analysis

Primary AML cells were harvested after treated with DMSO or PRLi (10 μM) for 24 hours. Wash once in PBS. Add cold 70% ethanol drop wise to the pellet while vertexing and fix for 30 min at 4°C. Wash twice in PBS and spin at 850 g in a centrifuge and be careful to avoid cell loss when discarding the supernatant especially after spinning out of ethanol. Add 50 μl of a 100 μg/ml stock of RNase to avoid RNA. Add 200 μl PI (from 50 μg/ml stock solution) in each sample and incubate 15 minutes at room temperature. Wash once in PBS then perform flowcytometry analysis. Experiments were performed on FACS LSR IV cytometers (BD Biosciences) and analyzed by using the FlowJo_v10 software.

Apoptosis assays

Primary AML cells were harvested after treated with DMSO or PRLi (10 μM) for 24 hours. Wash once in PBS. Resuspend cells in 1X Binding Buffer Solution at a final concentration of 1 x 10^6 cells/ml. To each 100 μL of cell suspension, add 5 μL of Annexin V and 5 μL of Propidium Iodide Staining Solution. Incubate cells at room temperature for 15 minutes avoiding the light. Add 400 μL of 1X Binding Buffer Solution. Experiments were performed on FACS LSR IV cytometers (BD Biosciences) and analyzed by using the FlowJo_v10 software.

Co-Immunofluorescence

HA-CBL was co-transfected with GFP-PRL2 in U2OS cells. 24 h after transfection, U2OS cells and MV-4-11 cells were fixed with 4% paraformaldehyde in phosphate-buffered saline (PBS) for 15 min at room temperature, permeabilized with 0.2% Triton X-100 in PBS for 10 min and blocked with BSA. Anti-HA antibody was applied to U2OS cells and Anti-CBL and anti-PRL2 antibodies were applied to MV-4-11 cells overnight at 4°C, followed by three times of washing with PBS and 1h incubation with goat anti-mouse alexa fluor 555 secondary antibody. After washing with PBS, the coverslips were mounted with

VECTASHIELD® PLUS Antifade Mounting Medium with DAPI (Vector Laboratories, H-2000-10). Images were obtained with a Nikon Inverted Microscope Eclipse Ti-S.

GST pull down assays

1 x 10^9 MV-4-11 cells were treated with 1 mM pervanadate for 30 minutes and collected by centrifugation. The cell pellet was lysed with 3 ml lysis buffer (20 mM Tris, pH 7.5, 100 mM NaCl, 1% Triton X-100, 10% glycerol, supplemented with 5 mM iodoacetic acid, 1 mM orthovanadate, and proteases inhibitors). 10 mM DTT was added in the lysate and incubated for 15 min on ice to inactivate any unreacted iodoacetic acid and pervanadate. Supernatant was collected by centrifugation at 14,000 g for 15 min. 25 μg GST, GST-PRL2 or GST-PRL2-CSDA were coupled to GST beads in lysis buffer, incubated at 4°C for 1h. Cell lysates were incubated with GST proteins conjugated to beads at 4 °C for 2h. The beads were pelleted and washed 3 times for 5 min with lysis buffer. Bound proteins were re-suspended in 50 μL Laemmli sample buffer, boiled for 5 min, and the samples are resolved by SDS-PAGE gels.

Immunoprecipitation (IP) assays

For Immunoprecipitation (IP), Cells were washed with ice-cold PBS and lysed on ice for 30 min in lysis buffer (50 mM Tris-HCl, pH 7.4, 150 mM NaCl, 1% Triton X-100, and 10% glycerol) supplemented with a Complete Protease and Phosphorylation Inhibitor tablet (Thermoscientific, A32961). Cell lysates were cleared by centrifugation at 15,000 rpm for 10 min. The lysate protein concentration was estimated using a BCA protein assay kit (Pierce). IP antibody plus Protein A Agarose beads (Sigma-Millipore) was added, and samples were incubated on shaker at 4 °C for overnight. After washing with lysis Buffer, the samples were ready for western blot analysis.

For the peroxidase APEX2 assay, HA-CBL or HA-CBL/Y371F were transiently expressed in 293 cells stably expressing APEX2-PRL2 with PEI. 48 h after transfection, biotin-phenol labeling was performed by changing the medium to fresh growth medium containing 2.5 mM biotin-phenol for 30 min at 37 °C

under 5% CO_2 according to previously published protocols.[44] Then, a final concentration of 0.5 mM H_2O_2 was added into the plate for 1 min. The reaction was then quenched by replacing the medium with 1X PBS containing 5 mM Trolox, 10 mM sodium ascorbate and 10 mM sodium azide. Cells were washed with PBS containing 5 mM Trolox, 10 mM sodium ascorbate and 10 mM sodium azide for three times and lysed with lysis buffer (50 mM Tris (pH 8.0), 150 mM NaCl, 10% Glycerol, 1% Triton-X-100) supplied with phosphatase inhibitor (Bimake, B15002) and protease inhibitor mixture (Roche Applied Science, 04693132001). Biotinylated proteins are enriched with neutravidin beads (Thermo Scientific, PI29202) and identified by Western blot.

For the Flag-PRL2-CSDA trapping assay, HA-CBL or HA-CBL/Y371F were transiently expressed in HEK293 cells or HeLa cells stably expressing Flag-PRL2-CSDA trapping mutant with PEI. 48 h after transfection, the cells were treated with 300 μM pervanadate for 30 min, then the medium was replaced with fresh medium for another 30 min, and the cells were washed for three time with PBS. Then the cells were lysed with 1 mL lysis buffer (50 mM Tris (pH 8.0), 150 mM NaCl, 10% Glycerol, 1% Triton-X-100) supplied with phosphatase inhibitor (Bimake, B15002) and protease inhibitor mixture (Roche Applied Science, 04693132001) on ice for 15 min and then spun at 14,000 rpm at 4 °C for 30 min, and the supernatant was transferred to a fresh tube and Flag agarose beads (Bimake, B23102) were added and incubated at 4 °C for 3 h. Beads were collected by centrifugation at 3,000 rpm for 1 min and the supernatant was removed. Beads were washed three times with 1 mL lysis buffer. Bound proteins were resuspended in 50 μL Laemmli sample buffer and boiled for 5 min, and the samples were resolved by SDS/PAGE and examined by Western blotting.

Sequencing data

Transcriptional expression data of PRL2 and all data on clinical, cytogenetic characteristics, and survival were derived from TCGA official website (https://www.cancer.gov/about-nci/organization/ccg/research/structural-genomics/tcga) or cBioPortal (https://www.cbioportal.org).

For RNA-seq assays in hematopoietic stem and progenitor cells (HSPCs), embryonic day 14.5 fetal liver cells were collected from *Prl2*$^{+/-}$ pregnancy female. Total RNA was isolated by MiniRNA universal kit. RNA-seq was performed by Genomic Core in Indiana University. Library was prepared by Clontech SMART-Seq v4 Ultra Low Input RNA Kit, Illumina Nextera XT DNA Lib Kit. and RNA-seq was performed on Illumina NovaSeq 6000 system (Illumina, Inc.). RNA-seq data was analyzed, and the raw data was deposited in NCBI GEO (GSE208136). The Limma package in R Studio (version 4.1.0, RStudio Team (2020) was used to identify the DEGs. P<0.05 and |log2 fold change (FC)|>1 was used as the cut-off criteria for volcano plot for clinic data and heat map for fetal liver sequencing data by R Studio. All the DEGs were used to do Gene-set enrichment analysis by GSEA v4.2.2 software (http://www.gsea-msigdb.org/gsea/index.jsp). For HSPC sequencing data, the DEGs (P<0.05 and |log2 fold change (FC)|>1) was used to construct PPI networks with an interaction score >0.4 by STRING (version 11.05).

Immunohistochemistry

Recipient mice repopulated with *Prl2*$^{+/+}$, *Prl2*$^{-/-}$, *Flt3*$^{+/ITD}$, *Flt3*$^{+/ITD}$*Prl2*$^{-/-}$, *Flt3*$^{ITD/ITD}$ and *Flt3*$^{ITD/ITD}$*Prl2*$^{-/-}$ BM cells mice were sacrificed at the same time. BM, liver, spleen, and PB were collected. Cellular morphology of PB smears were analyzed by May-Grünwald Giemsa staining. Bone, Liver and spleen section were stained with hematoxylin/eosin (H&E) at the Northwestern University (Chicago, IL). All slides were evaluated by conventional light–field microscopy using an optical microscope (Olympus, Japan).

Supplemental Figure Legends

Supplemental Figure 1.

(A) Relative *PRL2* (*PTP4A2*) mRNA expression in AML patients with or without CNS relapse.

(B) Overall survival of AML patients with high (n=71) or low (n=69) PRL2 expression.

(C) Overall survival of favorable cytogenetic risk AML patients with high (n=16) or low (n=15) *PRL2* expression.

(D) Overall survival of intermediate cytogenetic risk AML patients with high (n=38) or low (n=38) *PRL2* expression.

(E) Relative *PRL2* (*PTP4A2*) mRNA expression in AML patients with or without *FLT3* mutation, datasets are from cBioportal.

(F) Overall survival of *FLT3* mutation negative AML patients with high (n=49) or low (n=48) *PRL2* expression.

Supplemental Figure 2

(A) Quantitative RT-PCR analysis of gene expression in Kit^+ cells from E14.5 WT and *Prl2* null fetal liver (n=4).

(B) Image Lab software was used to calculate the gray value of each band. Graph showing the ratio of the relative density of phosphorylated protein/total protein expression and normalized with β-actin from WT and *Prl2* null fetal liver cells (n=3).

(C) Graph showing the ratio of the relative density of phosphorylated protein/total protein expression and normalized with β-actin from WT and *Prl2* bone marrow Lin^- cells (n=3).

(D) Prl2 deficiency decreased the proliferation of hematopoietic progenitor cells expressing MIGR1-FLT3-ITD (MSCV-FLT3-ITD-IRES-GFP) both in the absence of cytokines and in the presence of FLT3 ligand (n= 3).

(E) Wild-type FLT3 (MSCV-FLT3-IRES-GFP) or FLT3-ITD (MSCV-FLT3-ITD-IRES-GFP) were introduced into Lin^- cells purified from wild-type and PRL2 null mice. Loss of Prl2 decreased the colony formation of HSPCs expressing FLT3-ITD (n = 3). CFU-M: Colony forming unit-macrophages, CFU-G: Colony forming unit-granulocytes, CFU-GM: Colony forming unit-granulocytes/ macrophages.

Mean values (±SEM) are shown (*$p<0.05$, **$p<0.01$, and ***$p<0.001$).

Supplemental Figure 3

(A) Representative body size of *Prl2*$^{+/+}$, *Prl2*$^{-/-}$, *Flt3*$^{+/ITD}$, *Flt3*$^{+/ITD}$*Prl2*$^{-/-}$, *Flt3*$^{ITD/ITD}$ and *Flt3*$^{ITD/ITD}$*Prl2*$^{-/-}$ mice.

(B-H) White blood cell (WBC), red blood cell (RBC), hemoglobin (HGB), platelet, basophil, monocyte, and eosinophil count in peripheral blood (PB) of *Prl2*$^{+/+}$, *Prl2*$^{-/-}$, *Flt3*$^{+/ITD}$, *Flt3*$^{+/ITD}$*Prl2*$^{-/-}$, *Flt3*$^{ITD/ITD}$ and *Flt3*$^{ITD/ITD}$*Prl2*$^{-/-}$ mice (n=8 mice per group).

(I) The frequency of myeloid cells, B cells and T cells in PB of *Prl2*$^{+/+}$, *Prl2*$^{-/-}$, *Flt3*$^{+/ITD}$, *Flt3*$^{+/ITD}$*Prl2*$^{-/-}$, *Flt3*$^{ITD/ITD}$ and *Flt3*$^{ITD/ITD}$*Prl2*$^{-/-}$ mice (n=8 mice per group).

(J) BM cellularity of *Prl2*$^{+/+}$, *Prl2*$^{-/-}$, *Flt3*$^{+/ITD}$, *Flt3*$^{+/ITD}$*Prl2*$^{-/-}$, *Flt3*$^{ITD/ITD}$ and *Flt3*$^{ITD/ITD}$*Prl2*$^{-/-}$ mice (n=6 mice per group).

(K-M) The frequency of myeloid, B, and T cells in the bone marrow of *Prl2*$^{+/+}$, *Prl2*$^{-/-}$, *Flt3*$^{+/ITD}$, *Flt3*$^{+/ITD}$*Prl2*$^{-/-}$, *Flt3*$^{ITD/ITD}$ and *Flt3*$^{ITD/ITD}$*Prl2*$^{-/-}$ mice (n=6 mice per group).

(N) The frequency of myeloid progenitor (MyePro) (Lin$^-$Sca1$^-$cKit$^+$), MEP (Lin$^-$Sca1$^-$cKit$^+$CD34$^-$CD16/32$^-$), CMP (Lin$^-$Sca1$^-$cKit$^+$CD34$^+$CD16/32$^-$), and GMP (Lin$^-$Sca1$^-$cKit$^+$CD34$^+$CD16/32$^+$) in the BM of *Prl2*$^{+/+}$, *Prl2*$^{-/-}$, *Flt3*$^{+/ITD}$, *Flt3*$^{+/ITD}$*Prl2*$^{-/-}$, *Flt3*$^{ITD/ITD}$ and *Flt3*$^{ITD/ITD}$*Prl2*$^{-/-}$ mice (n=6).

Mean values (±SEM) are shown (*p<0.05, **p<0.01, ***p < 0.001).

Supplemental Figure 4

(A) Experimental design of primary competitive BM transplantation assays.

(B-C) White blood cell (WBC), neutrophil, lymphocyte, and monocyte count in peripheral blood (PB) of primary transplantation recipient mice (n=8 mice per group).

(D) The frequency of donor derived myeloid progenitor (MyePro), MEP, CMP, and GMP in the BM of primary transplantation recipient mice (n=8 mice per group).

(E) Experimental design of secondary BM transplantation assays.

(F-G) WBC, neutrophil, lymphocyte, monocyte count in peripheral blood (PB) of the secondary transplantation recipient mice (n=8 mice per group).

(H) The frequency of donor derived myeloid progenitor (MyePro), MEP, CMP, and GMP in the BM of secondary transplantation recipient mice (n=8 mice per group).

(I-J) The size and weight of spleen of the secondary transplantation recipient mice (n=9-10 mice per group).

Mean values (±SEM) are shown (**p<0.01, ***p < 0.001, ****p < 0.0001).

Supplemental Figure 5

(A-G) RBC, HDB level, WBC, platelet, neutrophil, monocyte and basophil count in peripheral blood (PB) of recipient mice repopulated with $Prl2^{+/+}$, $Prl2^{-/-}$, $Flt3^{+/ITD}$, $Flt3^{+/ITD}Prl2^{-/-}$, $Flt3^{ITD/ITD}$ and $Flt3^{ITD/ITD}Prl2^{-/-}$ BM cells (n= 9-10).

(H) Representative H&E (10×) images of the peripheral blood smears, bone marrow, spleen, and liver of recipient mice repopulated with $Prl2^{+/+}$, $Prl2^{-/-}$, $Flt3^{+/ITD}$, $Flt3^{+/ITD}Prl2^{-/-}$, $Flt3^{ITD/ITD}$ and $Flt3^{ITD/ITD}Prl2^{-/-}$ BM cells.

Mean values (±SEM) are shown.

Supplemental Figure 6

(A) Western blot analysis for PRL2 in MOLM-13 and K562 cells transduced with lentiviruses expressing a control shRNA (shCtrl) or a PRL2 shRNA (shPRL2).

(B-C) Knocking down of PRL2 significantly decreased the colony formation of MOLM-13 and K562 cells (n=3). Representative images of the colonies are shown.

(D) Kaplan-Meier survival curve of sublethally irradiated NSG mice transplanted with $3x10^6$ MOLM-13 cells expressing shCtrl or shPRL2 (n=7 mice group).

(E-F) PRLi treatment significantly decreased the colony formation of MOLM-13 and K562 cells (n=3). Representative images of the colonies are shown.

(G) Colony formation of MV-4-11, MOLM-13, and K562 with or without genetic knock down of PRL2 treated with PRLi (n=3).

(H) Proliferation of MV-4-11 and MOLM-13 cells expressing GFP, PRL2, or PRL2-CSDA in the presence or the absence of PRLi (5 μM) (n=3).

(I) Cell cycle analysis of primary AML cells with FLT3-ITD mutation (AML3150) at 24 hours following DMSO or PRLi (10 μM) treatment.

(J) Apoptosis analysis of primary AML cells with FLT3-ITD (AML3150) at 24 hours following DMSO or PRLi (10 μM) treatment.

(K) Kaplan-Meier survival curve of NSG mice transplanted with 4 x 10^6 human $CD45^+$ leukemia cells (AML3242) following three weeks of DMSO or PRLi treatment (n=6 mice per group).

(L) Flow cytometry analysis of human $CD45^+$ cells in PB, BM, and spleen of NSG mice transplanted with 4 x 10^6 human $CD45^+$ leukemia cells (AML3242) after three weeks of DMSO or PRLi treatment (n=4 mice per group).

Supplemental Figure 7

(A) Representative western blot analysis of STAT3, STAT1 and MEK phosphorylation in MV-4-11 cells following dimethyl sulfoxide (DMSO) or PRLi treatment.

(B) Representative western blot analysis of FLT3, AKT, STAT5, STAT3, STAT1 and MEK phosphorylation in K562 cells following dimethyl sulfoxide (DMSO) or PRLi treatment.

(C) Representative western blot analysis of BCR-ABL, BCR, and c-ABL in K562 cells following DMSO or PRLi treatment.

(D) Representative western blot analysis of FLT3, AKT, STAT5 and ERK phosphorylation in U937 cells expressing WT FLT3 or FLT3-ITD following DMSO or PRLi treatment.

(E) Graph showing the ratio of the relative density of phosphorylated protein/total protein expression and normalized with β-actin in human $CD45^+$ cells in BM of NSG mice 4 weeks after transplanted with MV-4-11 cells expressing control shRNA or shPRL2 (Left panel, n=3 mice per group); in human

$CD45^+$ cells in BM of NSG mice transplanted with MV-4-11 cells following three weeks of DMSO or PRLi treatment (Middle panel, n=3 mice per group); and in human $CD45^+$ cells in BM of NSG mice transplanted with PDX cells (AML3179) following three weeks of DMSO or PRLi treatment (Right panel, n=3 mice per group).

(F) Representative western blot analysis of PTEN levels in MV-4-11 cells expressing shCtrl or shPRL2 (Up panel) or in MV-4-11 cells following DMSO or PRLi treatment (Bottom panel).

(G) MV-4-11 cell proliferation at 24 hours after PRLi (5 μM) and AC220 (2.5 nM) or PRLi (5 μM) and Gilteritinib (5nM) treatment.

Supplemental Figure 8

(A) PRLi treatment decreased FLT3 half-life in MV-4-11 cells.

(B) PRLi treatment enhanced FLT3 ubiquitination in MV-4-11 cells.

(C) Immunofluorescence analysis showed that PRL2 co-localizes with CBL in U2OS cells.

(D) Protein structure of CBL. CBL becomes phosphorylated at Y371, Y700, Y731, and Y774 following cytokine stimulation.

(E) Representative western blot analysis showed that PRLi treatment increases CBL phosphorylation at tyrosine 371 in MV-4-11 cells.

(F) The mRNA level of *PRL2* and *CBL* from AML were plotted and Spearman rank-correlation analyses were performed. *PRL2* expression is positively correlated with *CBL* expression in these AML samples from TCGA dataset.

Supplementary Figure 1

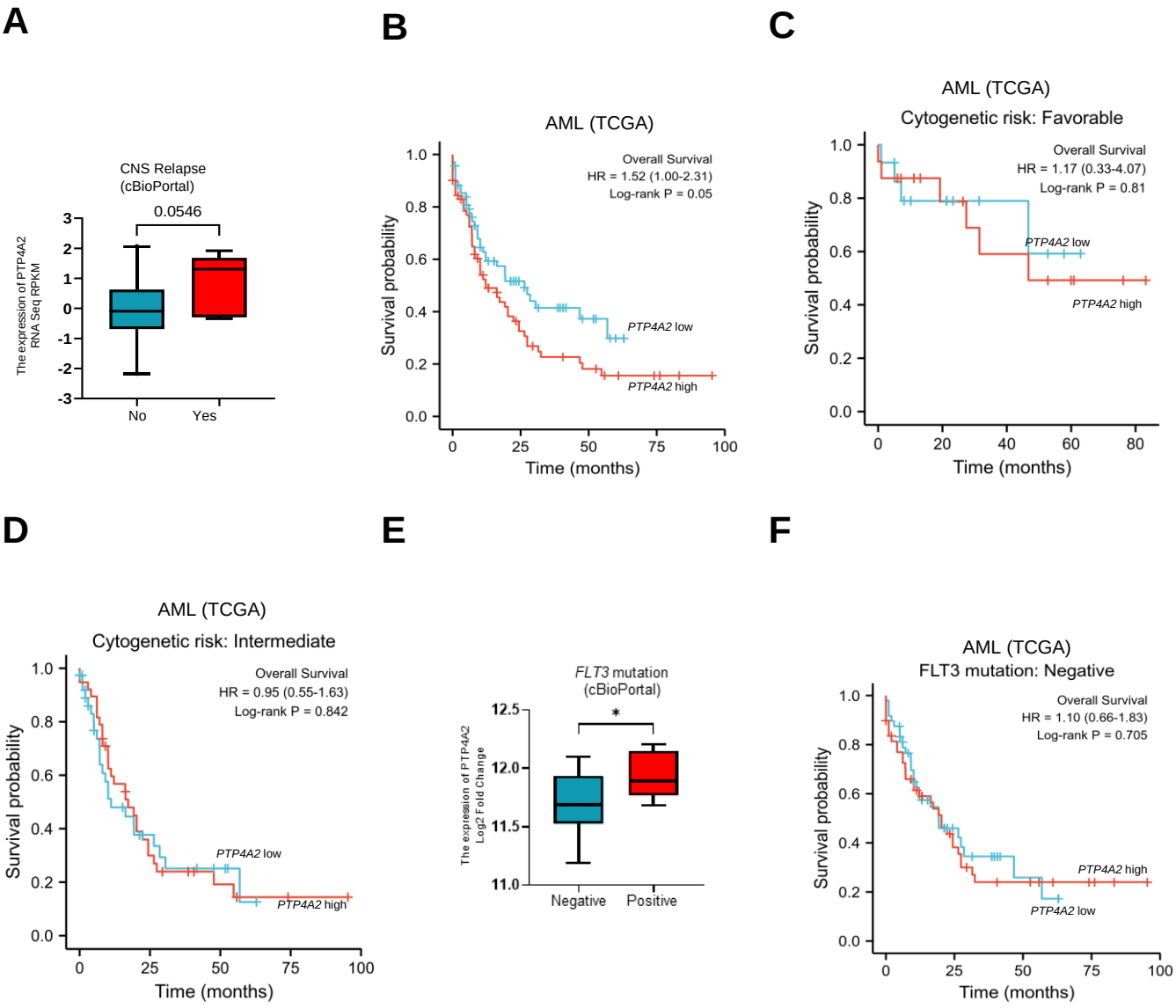

Supplementary Figure 2

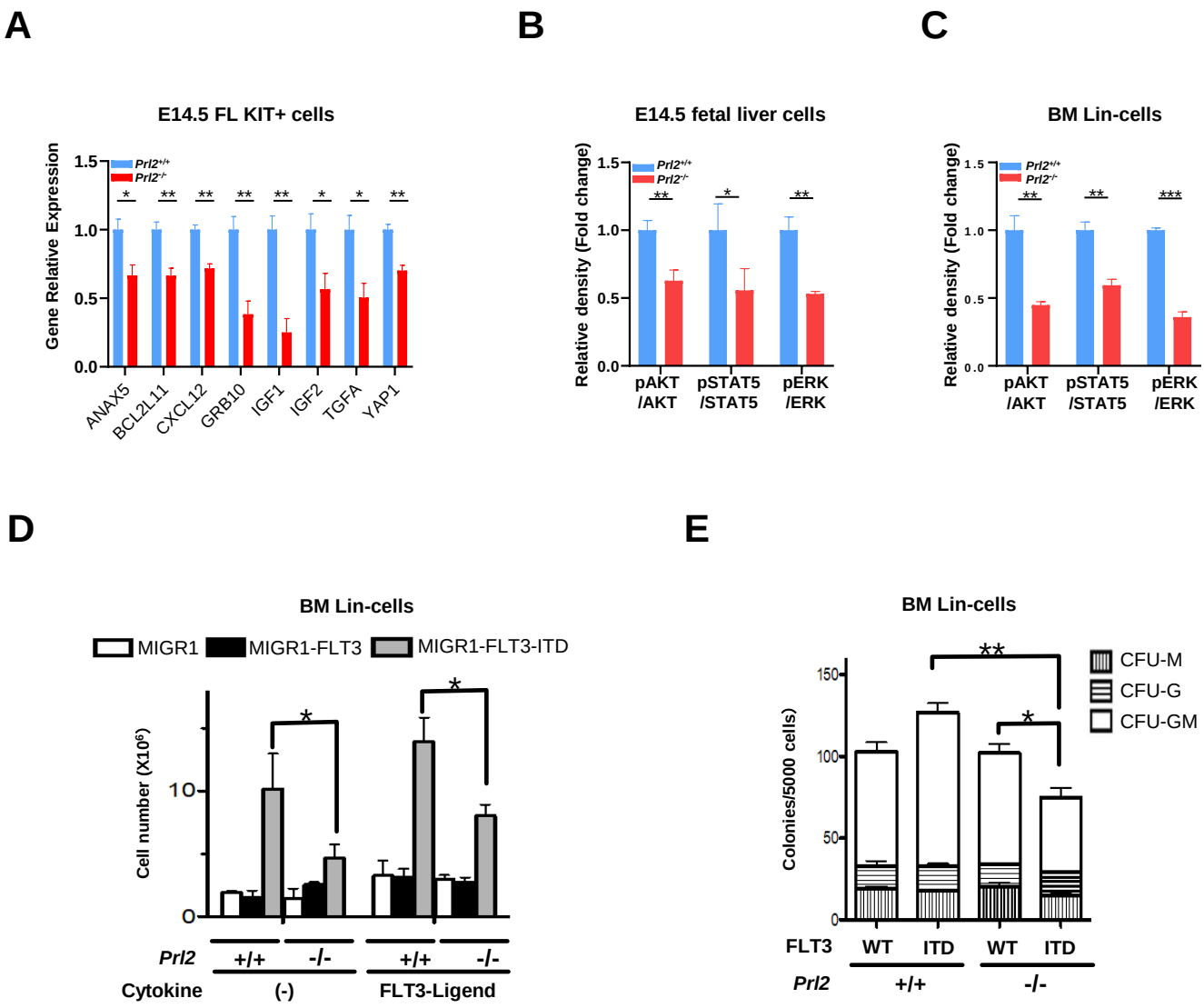

Supplementary Figure 3

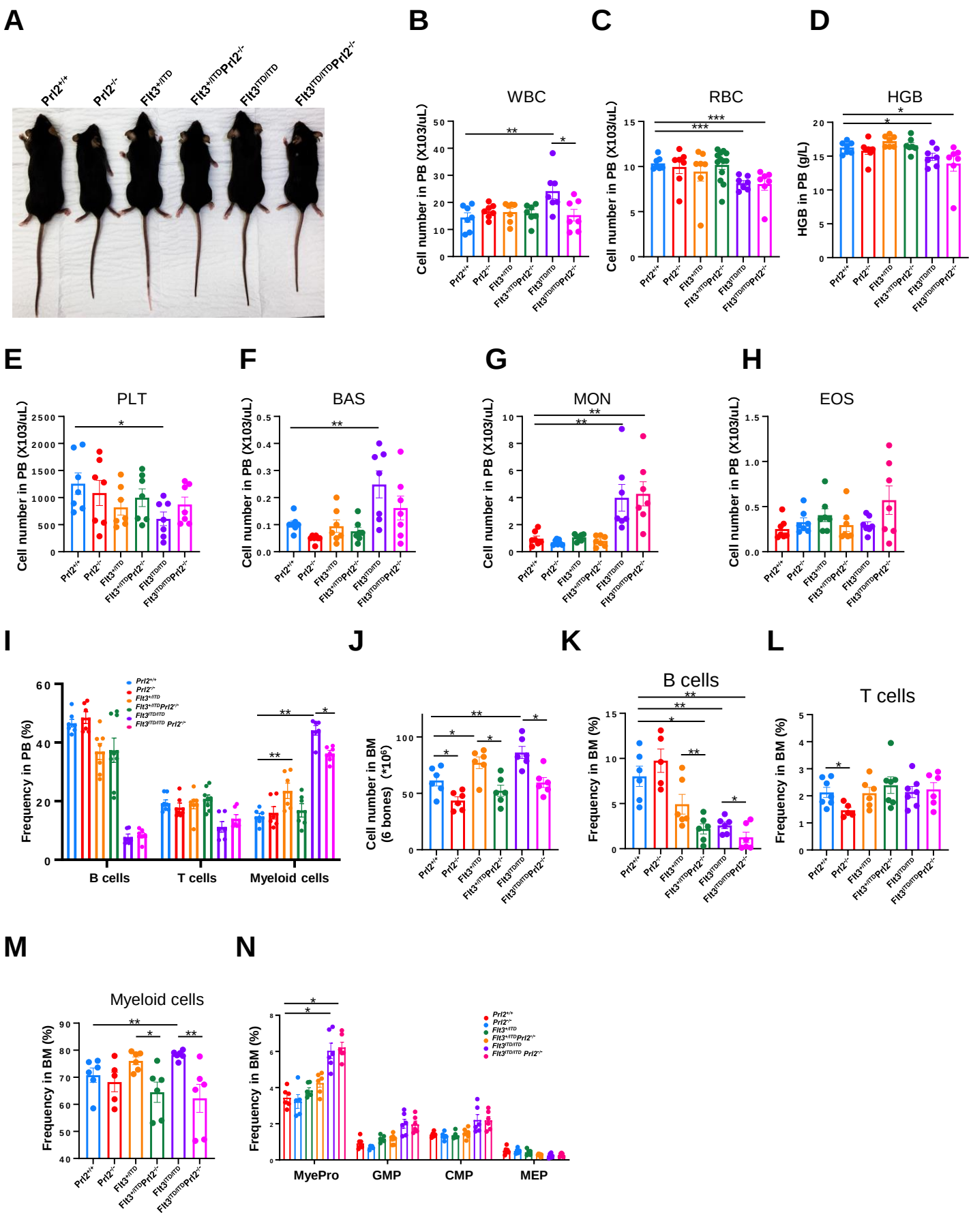

Supplementary Figure 4

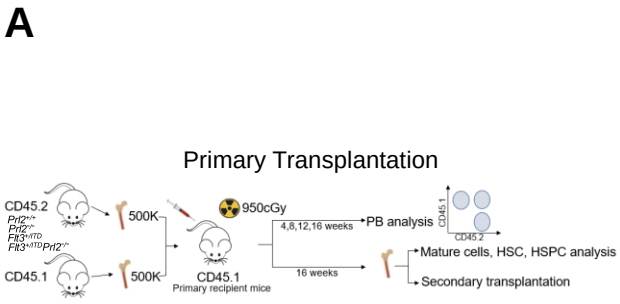

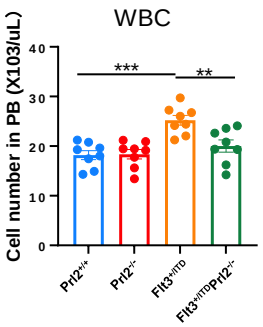

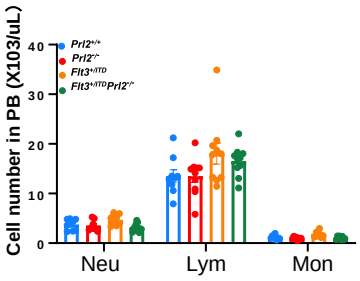

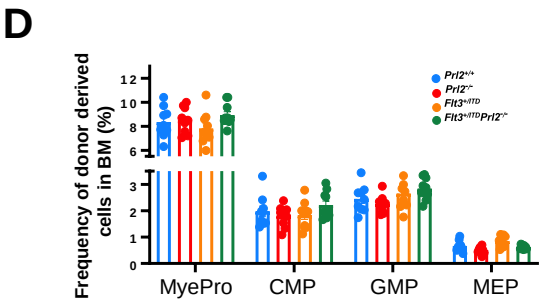

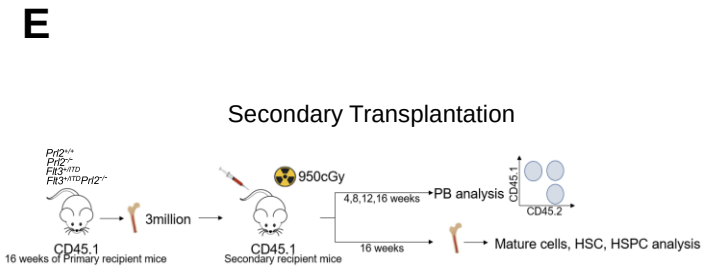

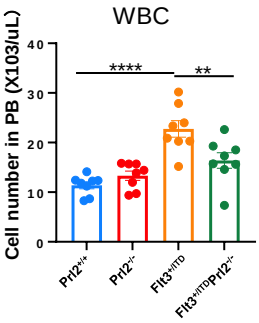

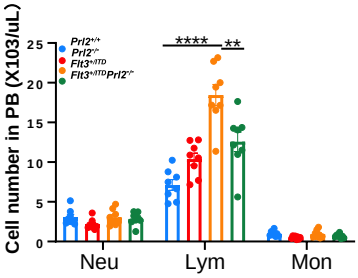

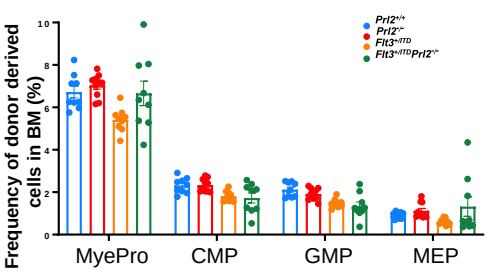

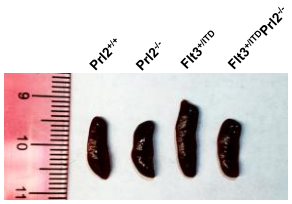

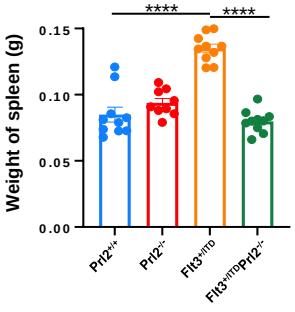

Supplementary Figure 5

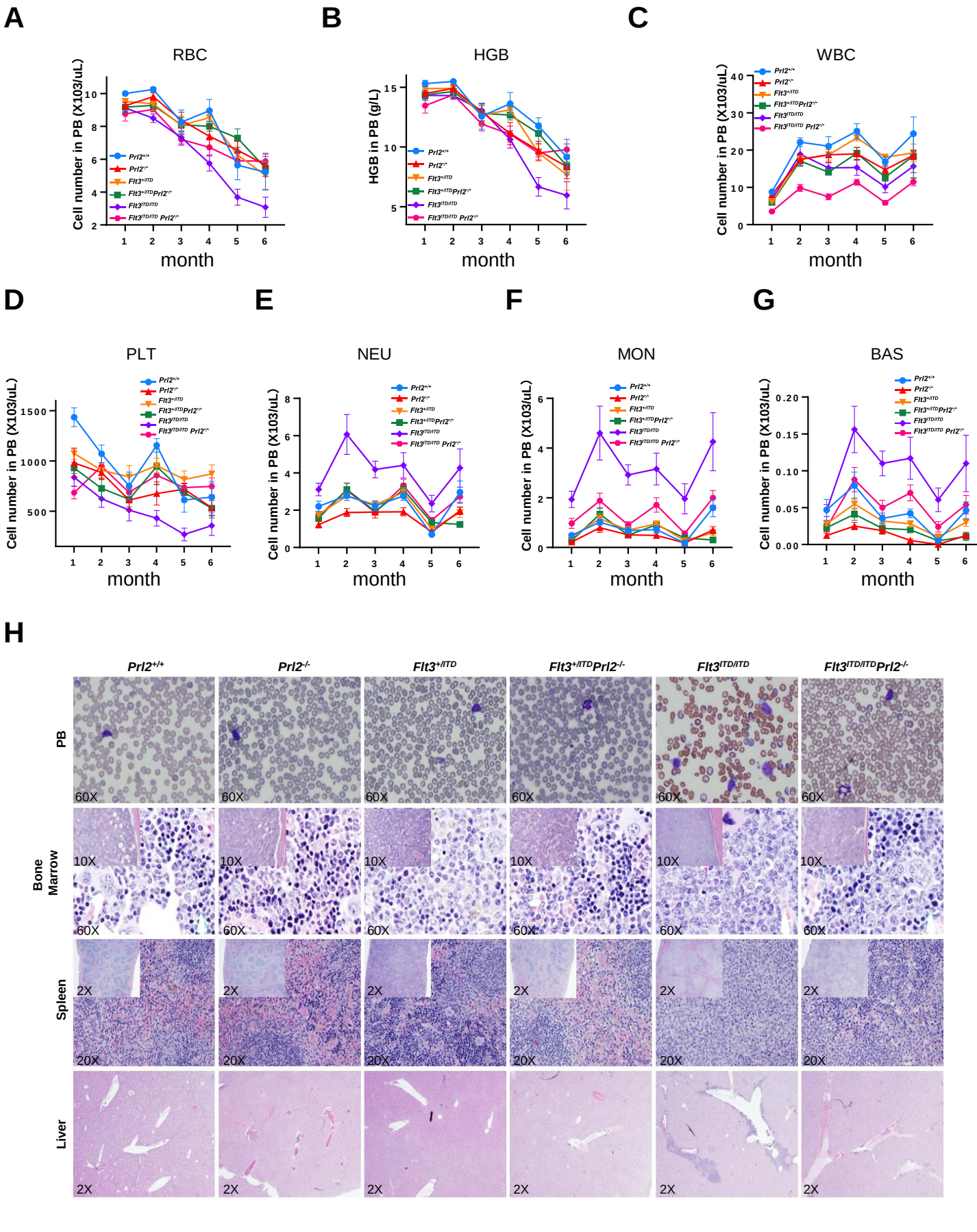

Supplementary Figure 6

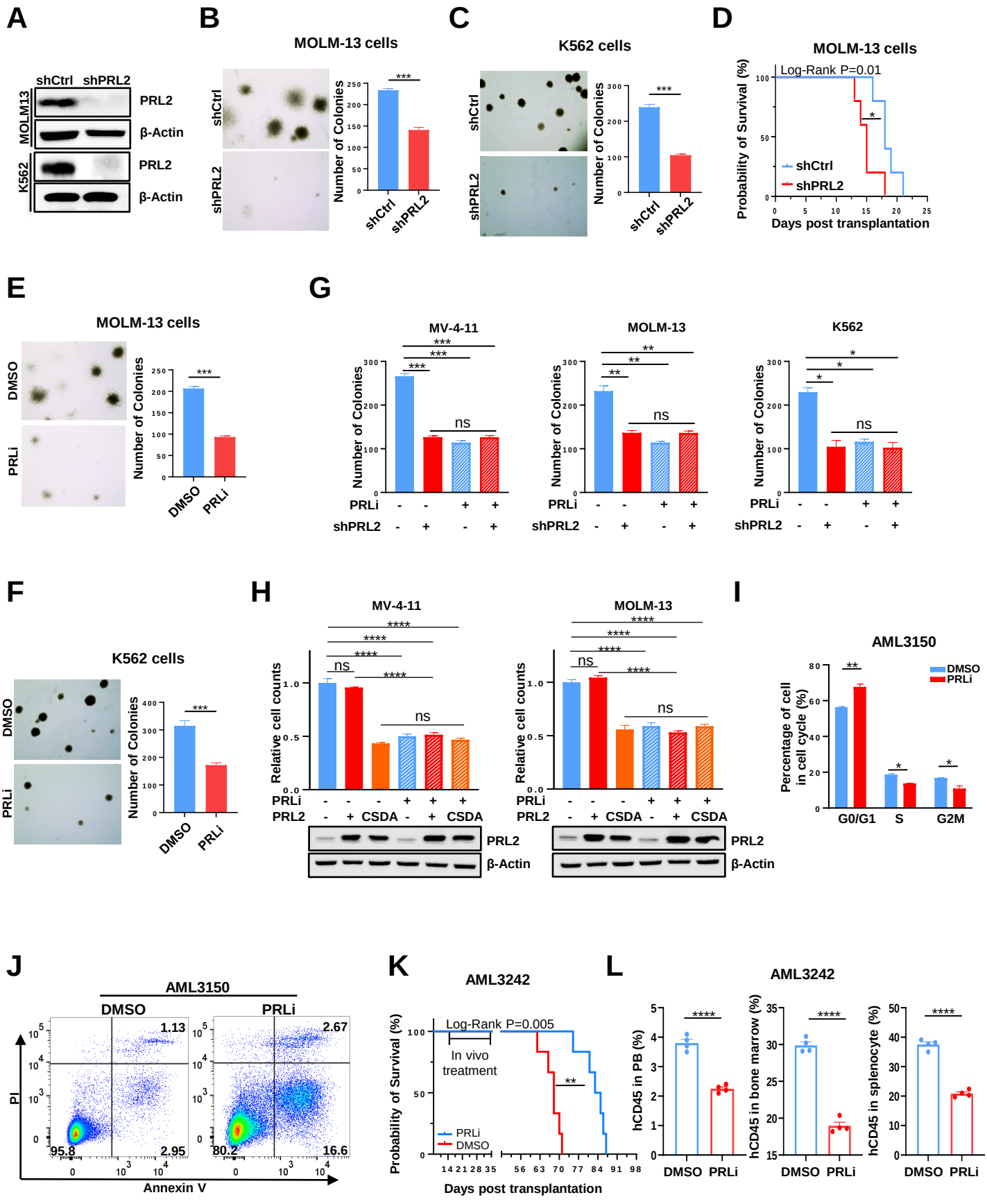

Supplementary Figure 7

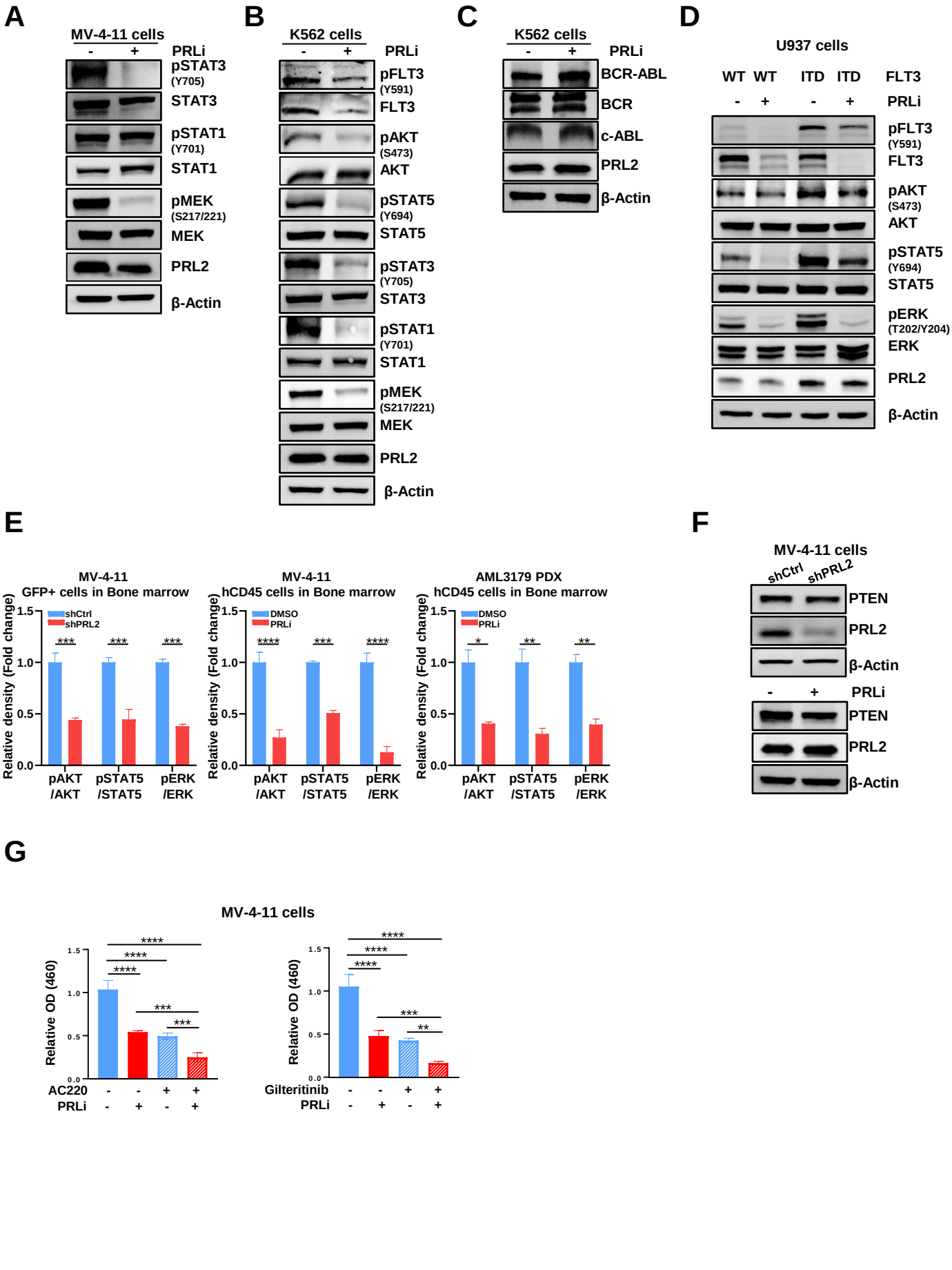

Supplementary Figure 8

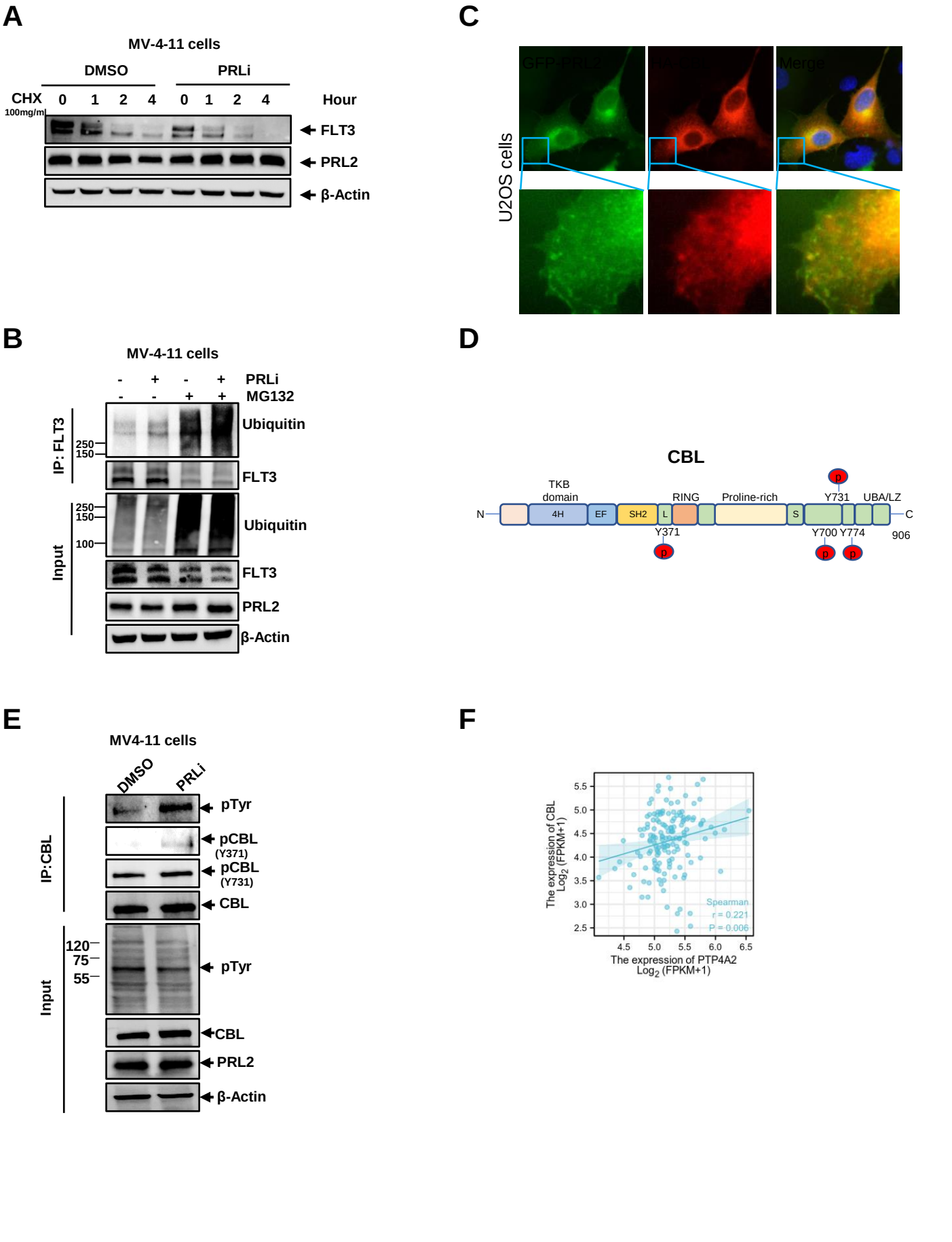

Supplementary Table 1. Clinical information relevant to AML patient samples

Sample#	Age	Sex	Sample type	Disease Status	Karyotype	Mutations	WBC
3142	56	F	BM	Relapse	t(12;15)[4] XX	FLT3-ITD	6.4K
3150	55	F	PB	Relapse	(46,XX)[20]//Donor (46,XY)[7]	FLT3-ITD	19.5K
3163	63	F	PB	New diagnosis	Normal karyotype	FLT3-ITD,NPM1	38K
3179	46	M	BM	Relapse	Normal karyotype	FLT3-ITD	31K
3220	33	F	BM	New diagnosis	Normal karyotype	KRAS,ASXL1,WT1, FLT3-ITD	69K
3242	56	F	BM	New diagnosis	Normal karyotype	FLT3-ITD,NPM1, PTPN11	81K
3080	37	F	BM	New diagnosis	Normal karyotype	FLT3-ITD	70K
3145	69	M	BM	New diagnosis	trisomy 8	FLT3-ITD	76K
3202	25	M	PB	New diagnosis	Normal karyotype	Negative Flt3 mutation	63k
3153	26	M	BM	Relapse	Complex	Negative Flt3 mutation	10K

BM= Bone Marrow; PB=Peripheral Blood

Supplementary Table 2. Key resources

Reagents or Resource	Source	Identifier
Western-Blot antibodies		
pAKT-S473	Cell signaling Technologies	9271
AKT	Cell signaling Technologies	4691S
pSTAT5-Y694	Cell signaling Technologies	9351
STAT5	Cell signaling Technologies	94205
pERK-T202/Y204	Cell signaling Technologies	9101
ERK	Cell signaling Technologies	9102
β-Actin	Cell signaling Technologies	3700
Ubiquitin	Cell signaling Technologies	3936
PLCy	Cell signaling Technologies	5690
SHP2	Cell signaling Technologies	3397
CBL-human	Cell signaling Technologies	8447s
CBL-Y774	Cell signaling Technologies	3555
CBL-Y731	Cell signaling Technologies	3554
CBL-Y700	Cell signaling Technologies	8869
FLT3	Cell signaling Technologies	3462S
pFLT3	Cell signaling Technologies	3464
pSTAT3-Y705	Cell signaling Technologies	9145S
STAT3	Cell signaling Technologies	12640S
pSTAT1-Y701	Cell signaling Technologies	9167S
STAT1	Cell signaling Technologies	14994S
pMEK-Y217/221	Cell signaling Technologies	9154S
MEK	Cell signaling Technologies	4694S
Anti-mouse IgG, HRP-linked Antibody	Cell signaling Technologies	7076
Anti-rabbit IgG, HRP-linked Antibody	Cell signaling Technologies	7074
PRL2	Sigma Aldrich	05-1583
pTyr	Sigma Aldrich	05-321
CBL-Y371	Syed Feroj Ahmed et al., 2021	
CBL-mouse	Transduction	C40320
Flow Cytometry antibodies		
FITC anti-mouse/human CD45R/B220 Antibody	biolegend	103206
PE/Cy7 anti-mouse CD3ε Antibody (100 µg)	biolegend	100320
APC/Cy7 anti-mouse/human CD11b Antibody	biolegend	101226
PerCP/Cyanine5.5 anti-mouse Gr-1 Antibody	biolegend	108428
APC anti-mouse CD45.2 Antibody	biolegend	109814
PE anti-mouse CD45.1 Antibody	biolegend	110708
APC/Cy7 Streptavidin	biolegend	405208
Pacific Blue™ anti-mouse Sca-1 Antibody	biolegend	108120
PE/Cy7 anti-mouse CD117 (c-Kit) Antibody	biolegend	105814
PerCP/Cy5.5 anti-mouse CD150 Antibody	biolegend	115922
APC anti-mouse CD48 Antibody	biolegend	103412
FITC anti-mouse CD45.2 Antibody	biolegend	109806
APC/Cy7 Streptavidin	biolegend	405208
PerCP/Cyanine5.5 anti-mouse Sca-1 Antibody	biolegend	108124
PE anti-mouse CD117 (c-Kit) Antibody	biolegend	105808
antimouse CD34 APC	biolegend	128612
PE/Cy7 anti-mouse CD16/32 Antibody	biolegend	101318
Pacific Blue™ anti-mouse CD45.1 Antibody	biolegend	110722
Biotin anti-mouse Lineage Panel	biolegend	133307
PE Anti-mouse CD45	biolegend	103105
BD Pharmingen™ APC Mouse Anti-Human CD45	BD Biosciences	555485

Continue to Supplementary Table 2. Key resources

Reagents or Resource	Source	Identifier
Chemicals, Culture medium		
PRLi (Cmpd43)	Yunpeng et al. (2016)	
RIPA buffer	Sigma-Aldrich	R0278
RBC lysis buffer	Biolegend	420302
Fetal Bovine Serum	GeminiBio	100-106
Antibiotic-Antimycotic	Gibco™	15240062
MethoCult™ GF M3434	Stem cell tech	M3434
MethoCult™ GF H4435	Stem cell tech	H4435
Critical commercial assays		
PureLink™ HiPure Plasmid Maxiprep Kit	Life tech corp	K210007
DNeasy Blood & Tissue Kit (50)	Qiagen	69504
MiniRNA universal kit	Qiagen	74134
MicroRNA universal kit	Qiagen	74034
FastStart Universal SYBR Green Master (Rox)	Sigma-Aldrich	4913850001
SuperScript™ IV First-Strand Synthesis System	invitrogen	18091200
Mouse Lin-cell depletion kit	Miltenyi Biotec	130-090-858
Human CD45 cell enrichment kit	Miltenyi Biotec	130-104-694
Mouse Kit+ cell selection kit	Miltenyi Biotec	130-091-224
Cell cycle kit	Abcam	ab139418
Apoptosis kit	Abcam	ab214485
Cell Proliferation Reagent WST-1	Sigma-Aldrich	11644807001
Deposited data		
RNA-seq data	Klein HU et al., 2009	GEO:GSE15434
RNA-seq data	This paper	GEO:GSE208136
TCGA	The Cancer Genome Atlas Program	https://www.cancer.gov/tcga
cBioPortal	Cerami et al., 2012 & Gao et al., 2013	https://www.cbioportal.org/
Software		
Gene set enrichment analysis	Subramanian et al. (2005)	https://www.gsea-msigdb.org/gsea/index.jsp
Rstudio 4.1.0	RStudio Team (2020)	http://www.rstudio.com/
GraphPad Prism 9	GraphPad	https://www.graphpad.com/
FlowJo_v10	BD Life Sciences	https://www.flowjo.com/solutions/flowjo/
Image J	Schneider et al., 2012	https://imagej.nih.gov/ij/
Experimental Models: Cell Lines		
MV-4-11	ATCC	CRL-9591
K562	ATCC	CCL-243
32D	ATCC	CRL-11346
293	ATCC	CRL-1573
U937	ATCC	CRL-1593.2
MOLM-13	Accegen Biotechnology	ABC-TC517S
Experimental Models: Organisms/Strains		
NOD-scid IL2Rgnull-3/GM/SF(NSGS)	The Jackson Laboratory	#013062
NOD.Cg-Prkdcscid Il2rgtm1Wjl/SzJ (NSG)	The Jackson Laboratory	#005557
B6.SJL(CD45.1+)	The Jackson Laboratory	#002014
C57BL/6 (CD45.2+)	The Jackson Laboratory	#000664
C3H/HeJ	The Jackson Laboratory	#000659